

Review

Engineering Heterostructures of Layered Double Hydroxides and Metal Nanoparticles for Plasmon-Enhanced Catalysis

Diana Gilea ^{1,2}, Radu G. Ciocarlan ², Elena M. Seftel ³, Pegie Cool ^{2,*}  and Gabriela Carja ^{1,*}

¹ Department of Chemical Engineering, Faculty of Chemical Engineering and Environmental Protection Technical University “Gh. Asachi” of Iasi, Bd. D. Mangeron, 700554 Iasi, Romania

² Laboratory of Adsorption and Catalysis (LADCA), Department of Chemistry, University of Antwerp, Universiteitsplein 1, 2610 Wilrijk, Belgium

³ Department of Sustainable Materials, VITO Flemish Institute for Technological Research, Boeretang 200, 2400 Mol, Belgium

* Correspondence: pegie.cool@uantwerpen.be (P.C.); carja@uaic.ro (G.C.);
Tel.: +32 (0)3-265-23-55 (P.C.); +40-232-278-683 (G.C.)

Abstract: Artificially designed heterostructures formed by close conjunctions of plasmonic metal nanoparticles (PNPs) and non-plasmonic (2D) lamellar nanostructures are receiving extensive interest. The synergistic interactions of the nanounits induce the manifestation of localized surface plasmon resonance (LSPR) in plasmonic metals in the specific environment of the 2D-light absorbing matrix, impacting their potential in plasmon enhanced catalysis. Specifically, layered double hydroxides (LDH) with the advantages of their unique 2D-layered structure, tuned optical absorption, ease of preparation, composition diversity, and high surface area, have emerged as very promising candidates for obtaining versatile and robust catalysts. In this review, we cover the available PNPs/LDH heterostructures, from the most used noble-metals plasmonic of Au and Ag to the novel non-noble-metals plasmonic of Cu and Ni, mainly focusing on their synthesis strategies toward establishing a synergistic response in the coupled nanounits and relevant applications in plasmonic catalysis. First, the structure–properties relationship in LDH, establishing the desirable features of the 2D-layered matrix facilitating photocatalysis, is shortly described. Then, we address the recent research interests toward fabrication strategies for PNPs/support heterostructures as plasmonic catalysts. Next, we highlight the synthesis strategies for available PNPs/LDH heterostructures, how these are entangled with characteristics that enable the manifestation of the plasmon-induced charge separation effect (PICS), co-catalytic effect, or nanoantenna effect in plasmonic catalysis with applications in energy related and environmental photocatalysis. Finally, some perspectives on the challenges and future directions of PNPs/LDHs heterostructures to improve their performance as plasmonic catalysts are discussed.

Keywords: layered double hydroxides; plasmonic nanoparticles; hybrid plasmonic catalysis



Citation: Gilea, D.; Ciocarlan, R.G.; Seftel, E.M.; Cool, P.; Carja, G. Engineering Heterostructures of Layered Double Hydroxides and Metal Nanoparticles for Plasmon-Enhanced Catalysis. *Catalysts* **2022**, *12*, 1210. <https://doi.org/10.3390/catal12101210>

Academic Editor: Xuming Zhang

Received: 13 September 2022

Accepted: 30 September 2022

Published: 11 October 2022

Publisher’s Note: MDPI stays neutral with regard to jurisdictional claims in published maps and institutional affiliations.



Copyright: © 2022 by the authors. Licensee MDPI, Basel, Switzerland. This article is an open access article distributed under the terms and conditions of the Creative Commons Attribution (CC BY) license (<https://creativecommons.org/licenses/by/4.0/>).

1. Introduction

Hybrid Plasmonic toward Optimized Photothermal-Photocatalytic Performances

Solar-to-chemical energy conversion by plasmon-driven photocatalysis is one of the sustainable approaches for obtaining intense electric fields, highly energetic electrons and local heating as tools to develop performant solutions to efficiently solve the environment pollution and improve the usage of solar energy. Among various promising routes, plasmonic hybrid nanocatalysts feature prominent solar driven surface plasmon resonance (SPR) [1]. SPR is related to the collective oscillations of the conduction electrons in metals and it can be classified into two modes: propagating surface plasmons (PSP) and localized surface plasmons (LSPR) [2].

By engineering the LSPR responses on a catalyst-molecule interface, a surface electronic state with an optimized energy can be created to selectively modulate solar-to-

chemistry conversion capabilities in catalytic processes [3,4]. Recent investigations have shown that it is possible to broaden the functionality of LSPR characteristics in multicomponent catalysts formed by close conjunctions of a plasmonic nanounit, which amplifies and concentrates the photons energy within the material, and a non-plasmonic nanocomponent that is able to play the role as support and, furthermore, to extract the plasmon energy in the form of electronic excitations to perform a targeted catalytic function [5]. On such a plasmonic/non-plasmonic interface the light energy harvested by the plasmonic metal can modulate specific interactions (MSI) with the support [6,7] that are entangled with the rearrangement of electrons, transfer of photogenerated carriers and their prolonged lifetime, and the extended light-response range [8] within heterostructured components. Moreover, the photogenerated carriers can promote shorter diffusion length with less recombination probability and enable superior photo-thermal-photocatalytic performances [9,10].

Currently, examples of heterostructured plasmonic photocatalysts include plasmonic-metal/metal [11] plasmonic-metal/2-D materials [12], plasmonic metal/carbon-based nanostructures [13], plasmonic metal/ metal-organic frameworks (MOFs) [14], or plasmonic-metal/molecule systems [9,15–17].

Based on these premises, this review presents the recent advancements in the synthesis, properties, and selective applications of metal plasmon-layered double hydroxides hybrids obtained by the close junction of plasmonic metal nanoparticles (PNPs) and 2D layered double hydroxides (LDH). The review starts by describing brief knowledge about layered double hydroxides as light absorbers facilitating photocatalysis, including information about the advantages of their 2D-layered structure showing a “memory effect”, specific mesoporous nanoarchitectonics, high stability, ease of preparation, and surface functionalities [18]. Next, the fundamentals of SPR are very shortly described, and we generally discuss noble and non-noble metals plasmonic heterostructures, which are applicable in diverse photocatalytic processes. Thereafter, here is provided a comprehensive overview of recent developments describing the current trends in design and fabrication strategies of PNPs/LDH heterostructures and how the synthesis can induce plasmonic catalysis by triggering the plasmon-induced charge separation effect (PICS), co-catalytic [19] effect, or antenna effect [20]. Finally, the review will provide some relevant examples in photocatalysis for energy related processes (e.g., water splitting, CO₂ reduction or alcohol production) and environmental processes (e.g., pollutants degradation and removal). Final remarks and outlook are given in the Conclusions.

2. 2-D Nanoarchitectures of Layered Double Hydroxides as Light Absorbers

Layered double hydroxides materials are a class of anionic clays with well-defined 2D lamellar structures and special characteristics, which makes them very attractive for many applications, e.g., as stable and recyclable adsorbents, heterogeneous catalysts, or catalyst supports for a variety of reactions with high industrial and academic importance. LDH-type materials are recognized to provide eco-friendly and low-cost solutions for today’s problems related to pollution or energy requirements [21]. Most of the LDH are synthetic and relatively simple and cheap to prepare on both the laboratory and industrial scale, respectively [22,23].

LDH are conventionally described by the general formula $[M^{II}_{1-x}M^{III}_x(OH)_2]^{x+} \cdot A^{n-}_{x/n} \cdot mH_2O$, where the divalent M^{II} and trivalent M^{III} cations may be Mg^{2+} , Zn^{2+} , Ni^{2+} , Cu^{2+} , Al^{3+} , Fe^{3+} , etc., and the A^{n-} can be almost any organic or inorganic anion [24,25]. LDHs may also be composed of M^I or M^{IV} , for example, Li^+ [26,27] or Ti^{4+} [28,29], Sn^{4+} [30,31], respectively. In such structures, the metallic cations are octahedrally coordinated to hydroxyl ions and form infinite layers of edge-shared MO_6 units. The hydroxylated layers are stacking one on top of each other in a 2D structure (Figure 1).

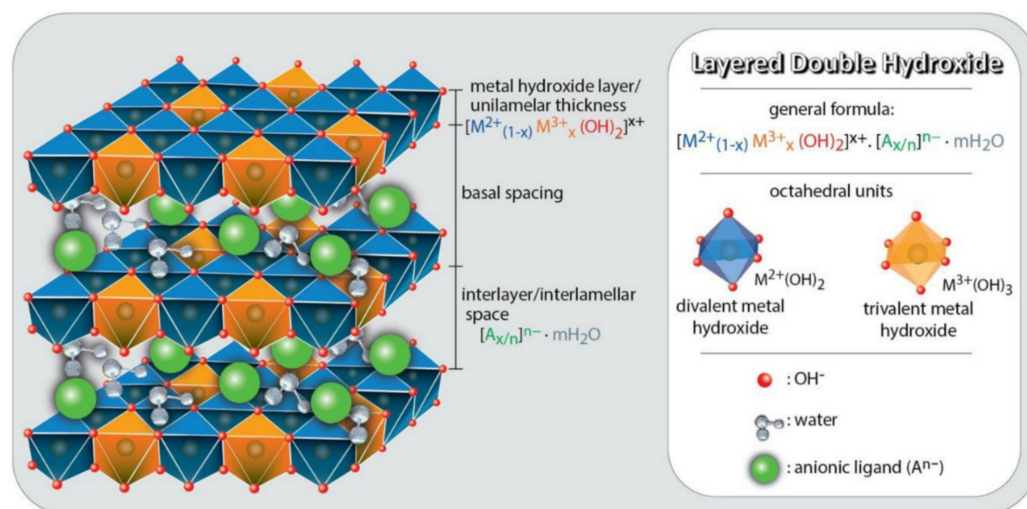


Figure 1. Schematic illustration of the chemical composition and structure of layered double hydroxides (LDHs) (Reprinted from [32] with permission of Elsevier, 2022).

Considerable research efforts are continuously realized into the design of different LDH-type structures for photocatalytic purposes due to their unique properties, i.e., their great adsorption capacity, which may be extended to visible light absorption via compositional variation, well dispersed MO_6 units, and O-H surface bonds that can react with holes of valence bands to produce hydroxyl radicals, unique layered morphology and high specific surface area, possibility of transformation to mixed metal oxide special structures and unique memory effect features, and last but not least, the availability of cheap and scalable synthesis procedures. All these valuable features indicate their advantageous application as photocatalytic materials (in the form of non-calcined LDH, mixed metal oxides, or as supports in hybrid nano-assemblies) for various applications, such as in renewable energy production and storage (water splitting, CO_2 reduction, alcohol photo reforming, batteries) [12,33–35] or pollutant degradation/removal in wastewater management [36–43].

LDH allow a very flexible choice in the nature of the metallic cations type to be inserted in the brucite-like sheets, resulting in binary, ternary, or multicomponent LDH, which together with the facile exchangeability of intercalated anions, facilitate their nanoscale tailoring for boosting the photocatalytic reactions. The cations in the MO_6 octahedral units are distributed in a uniform manner without clustering, offering a good metal dispersion, facilitating a wider separation of the electron–holes pairs, and thus, enhancing the photocatalytic activity by reducing the recombination. The combination of widely dispersed octahedral units sharing edges in a specific configuration in LDHs with variation of the nature of the metallic cations specifically identified as active in photocatalytic processes is of high importance. Various photocatalytic functionalities can be introduced by the isomorphous substitution of key metallic cations, as these can act as light absorbers and/or co-catalysts. In this context, the maximization of light harvesting (with extension to visible light) can be mentioned to generate sufficient energetic electrons and holes with high mobility, suppressing their bulk recombination and allowing sufficiently strong redox power to induce the targeted reactions. The effect is similar as the one achieved by coupling semiconductor nanoparticles having different band gap positions [44–47]. By tuning the LDH composition, the newly developed LDH materials may be regarded as nano assemblies of semiconductor nanoparticles where the advantageous layered network provides highly distributed metal cations in which the contact between the semiconductor active centers/sites is realized at the atomic level rather than at the particle level. This is of particular importance, as such highly uniformly dispersed catalytic active sites are not easily obtained in practice, where the control of homogeneity, consistency, and reproducibility is still a major issue, even at the laboratory scale.

Many research reports are demonstrating the importance of the mixed metal oxides derived from LDH structure as highly efficient photocatalysts as well as photocatalytic

supports. The unique memory effect property is advantageously employed in heterostructuring of nanoparticles, e.g., of metals (PNPs) or oxides, stabilizing the PNPs onto the LDH surface or in the interlayer, controlling their morphology. The obtained heterostructures show the synergistic effects of the individual nano-units, with modified electronic structure, enhancement of light harvesting and improved photocatalytic efficiency [12,43].

As mentioned above, an important strategy of shifting the photoresponsive properties of the LDH-type materials and harvesting the visible light is to isomorphously insert key cations, e.g., Cu^{2+} , Co^{2+} , Ni^{2+} , Fe^{3+} , Cr^{3+} or Y^{3+} within the hydroxylic 2D [35,46–48]. ZnCr-LDH is recognized for its potential of harvesting visible light irradiation [34,49]. Further, the hybridization of ZnCr-LDH with Au PNPs was reported to promote the degradation of gaseous volatile organic compounds and the nano-structuring of AuPNPs onto the LDH surface increased the photodegradation efficiency under visible light up to 83.6% [42]. Zhong-zhu Yang et al. describe that, in water splitting reactions, the transition metal-LDH or its nanocomposite is spatially separating the oxidation and reduction reaction sites due to the presence of both anions and cations in LDH which are both acting as reaction sites [47]. The tuning of the visible light absorption was also demonstrated for ternary LDHs composed of ZnCuAl or ZnCuGa [33] for which a red shift of their light absorption was observed. It was concluded that the insertion of Cu extended their absorption towards visible range based on the generation of an electronic state induced by Cu ions, leading to the narrowing of the LDH band gap. Furthermore, the same study, which focuses on the CO_2 conversion, reports that the insertion of Cu ions also influenced the selectivity towards methanol formation due to the fact that the Cu sites are also acting as binding sites for the CO_2 molecules, thus, interacting with the photogenerated electrons, protons and the $\text{Cu}^{\text{I}}/\text{Cu}^{\text{II}}$ redox couple. As a consequence, the CO_2 molecules undergo a series of reduction reactions, forming CH_3OH selectively. The narrow band gap is aligning with the redox level of $\text{CO}_2/\text{CH}_3\text{OH}$, which is favorable for the production of CH_3OH under light irradiation. CoAl-LDHs manifest also a narrowed band gap with consequent absorption in visible range. By measuring the UV-Vis absorption spectrum of CoAl LDH, it was demonstrated that the light absorption lies in the visible range and the photocatalyst has an estimated band gap of 2.1 eV [33]. Such a photocatalyst was used in the conversion of very low concentrations of atmospheric CO_2 and water to CH_4 [50]. The improved photocatalytic conversion and CH_4 generation was based on (i) the ability of to capture the visible light, (ii) the enhanced CO_2 adsorption by the surface OH groups, and (iii) the unique effect of divalent Co. Bai et al. studied the effect of the various cations (Mg^{2+} , Ni^{2+} , Co^{2+} , or Zn^{2+}) in the conversion of CO_2 under visible light irradiation and using the $[\text{Ru}(\text{bpy})_3]\text{Cl}_2 \cdot \text{H}_2\text{O}$ as photosensitizer. Among the studied photocatalysts, the CoAl-LDH exhibited the highest CO conversion rate and H_2 production, and the NiAl-LDH showed the highest CH_4 production due to the selectivity of Ni towards CH_4 . These photocatalytic performances were associated with (i) the improved light absorption and capturing the maximum of visible light region, (ii) the defects on the photocatalyst surfaces promoting CO_2 adsorption, and (iii) well matched energy levels of the LDH with the photosensitizer molecules, thus, under light irradiation, the photogenerated charges are drained towards the LDH surface where they can efficiently react with the adsorbed CO_2 [51].

The anions in LDH were demonstrated as having a positive influence also due to the effect on the LDH light absorption range, enlargement of the specific surface area, and modulating the interlayer spacing among the LDH layers, which improves the photocatalytic performance by facilitating the essential reaction between the reactants and the photoinduced charge carriers [52,53]. It was demonstrated that the interlayer space within the LDH layers act as an active site when Cu is present, such as in the situation when the CO_3^{2-} anions were exchanged with $[\text{Cu}(\text{OH})_4]^{2-}$ anions. An increased CO_2 conversion with selective CH_3OH formation was demonstrated when $[\text{Cu}(\text{OH})_4]^{2-}$ anions were intercalated, mainly assigned on the band gap narrowing and light absorption shifting after the intercalation of the $[\text{Cu}(\text{OH})_4]^{2-}$ anions [54]. Fluorine anions were found to enhance the photocatalytic activity based on the increased surface area of fluorinated LDH, while Cl^-

anions were demonstrated as acting as hole scavengers in a photocatalytic reduction of CO₂ using Cl intercalated NiAl-LDH, owing to the strong reducing character of Cl⁻ which is rapidly oxidized by holes, yielding HClO and selective formation of CO [55]. Intercalated organic anions, e.g., acetate anions, were also found to be advantageous in photocatalytic CO₂ conversion owing to the decomposition of the acetate anions absorbed on the LDH surface, which facilitates the electron transfer towards the CO₂ sites within the LDH [56].

In addition, the hydroxylated brucite-like layers are also advantageous for photocatalytic reactions. The surface-OH groups in LDH participate in the photocatalytic reactions in two different ways. First, the hydroxyl groups may be converted to hydroxyl radicals, which may be considered as the most effective reactive species responsible for photocatalysis [35,57]. Second, they may facilitate the formation of the ligand to metal charge transfer (LMCT) complexes on the surface of the semiconductor inorganic matrices, which favor the electron transfer and reduce the recombination, which promotes the process and enhances the photocatalytic efficiencies [58].

3. Heterostructures of Plasmonic Metal Nanoparticles/Support

3.1. Plasmon Excitation in Metal Nanoparticles

Certain metal nanoparticles own unique optical properties that lead to the manifestation of SPR. Essentially, there are two experimental signatures of SPR: propagating surface plasmons (PSP) and localized surface plasmons (LSPR). Herein, we define metal plasmon nanoparticles as nanoparticles of metals that interact with photons through an excitation of LSPR. LSPR concentrates electromagnetic fields to the surfaces and its relaxation processes lead to convert photon energy to energetic charge carriers or heat, which can be harvested in photocatalysis [59]. It was revealed that LSPR response (intensity) is a function of both the nature of the metal and the size/shape of the nanoparticles [60]. However, most PNPs suffer from instability, aggregation behavior, and susceptibility to various “poisoning” issues, limiting their use in catalysis through deactivation and poor reusability [61]. To address these challenges, heterostructures of plasmonic metals stabilized on a support is an important approach. The support has the role to confine and stabilize the PNPs and, furthermore, to modulate the evolving plasmonic energy within the heterostructure [62]. Notably, representative progress in the field points to the high impact of the synthesis strategies in establishing the characteristics associated with LSPR and MSI (metal–support interaction) in hybrid nanostructures [19].

In recent years, nanosized Au, Ag and Cu received most of the attention because they exhibit resonant behavior when interacting with ultraviolet and visible (UV-Vis) photons in the condition that a large fraction of light consists of UV-Vis photons. Additionally, non-noble PNPs (e.g., Ni) are newly emerging as an alternative to noble-metal-based ones due to their advantages, such as earth-abundance, cost effectiveness and application capabilities, and until now, they were investigated to a much lesser extent. Therefore, herein, we shortly point out some recent achievements regarding the fabrication of noble (Au, Ag) and non-noble (Cu, Ni) plasmonic nanoparticles/support heterostructures.

3.2. Heterostructures of Noble Plasmonic Metals/Support

Since they were discovered, noble plasmonic nanoparticles have attracted the attention of researchers from all over the world due to their special optical properties. Most studies were conducted on AuPNPs, AgPNPs, due to their unique features, such as great stability, simplicity in chemical synthesis, and controllable surface modification [63].

Wang et al. fabricated 0D/2D Au/TiO₂ in a two-step process. First, TiO₂ was prepared by a hydrothermal method and further decorated with AuNPs using the in situ growth method (Figure 2a). They obtained square-shaped TiO₂ nanosheets decorated with 5 nm size AuNPs recognized in the heterojunction. This type of 0D/2D heterojunction is ideal for separating photogenerated charges [64]. One-step synthesis was used by Kunthakudee et al. [60] to synthesize Au/TiO₂ with a simple photo-deposition method. They mixed commercial TiO₂ with a HAuCl₄ solution and irradiated it with UV-visible light. During the

irradiation, the temperature of the reaction was kept constant at 30 °C. A 0.5M NaOH solution was used to regulate the pH to the desired range (3.2–10). The obtained precipitate was separated by centrifugation, washed with water, and dried at 80 °C. The morphology showed semi-spherical AuNPs with a large average diameter of the particles. They proved that pH during the synthesis played a key role in tailoring the particle size of AuNPs, respectively, oxidation state. Thus, a decrease in the size of gold nanoparticles (from 34–77 nm to the range of 2.53–7.85 nm) was observed with increasing pH (from 3.2 to 10). Additionally, they found that at a lower pH (3.2), gold nanoparticles were deposited in metallic (Au⁰) and ionic (Au^{III}) states, while at higher pH (10) they were only in the metallic state [65]. Furthermore, Chang et al. reported the decoration of carbon nanorods (CN) and g-C₄N₃ by AuNPs using the hydrothermal reduction method. Primarily, they obtained carbon nanorods by the solvothermal method. Furthermore, the CN was mixed with an aqueous solution comprising the gold precursor (HAuCl₄) and glucose and stirred for 30 min. The obtained mixture was hydrothermally treated in an autoclave at 120 °C for 12 h. As final steps, centrifugation, washing with water, and drying of the precipitate were performed. Au/g-C₄N₃ was synthesized by the aforementioned method. The morphology after deposition showed a single CN decorated with approximately 13 nm diameter size AuNPs (Figure 2b). XPS measurements confirmed the presence of Au in the metallic state on the surface of CN and g-C₃N₄. UV–vis–NIR diffuse reflectance also confirmed the metallic state of AuNPs by the presence of the peak from 550 nm due to the LSPR effect of AuNPs [66]. An in situ method was used by Kashyap et al. to obtain AuNPs/CN nanosheets with high catalytic activity in Rhodamine B photodegradation. The CN nanosheets were obtained at 520 °C from urea with a 224 nm flake size. Spherical shaped AuNPs covering the CN nanosheets with a diameter 10.8 nm were noticed by HRTEM analysis. The XPS measurements revealed the presence of metallic Au⁰ and Au^{δ+} species. Due to the –OH adsorbed groups that bind with the oxidized Au⁺ species, the Au₂O was formed [67]. A novel type of support for plasmonic metal nanoparticles widely used in photocatalysis are metal-organic frameworks (MOFs). In comparison to more conventional materials such as zeolites and clays, MOFs perform better because they are a revolutionary type of porous material with tunable pore size, improved specific surface area, and outstanding porosity [68]. Thus, Liang et al. reported the immobilization of AuNPs on MIL-100(Fe) by a facile photodeposition method. They obtained homogeneously dispersed AuNPs on MIL-100(Fe) in the metallic state Au (0) with an average size diameter of 15 nm [69]. By the same method Cure et al. diffused ultra-small AuNPs (1 nm) into the MOFs (thiol-functionalized MOFs, including MIL-101 (Cr), MOF-808-SH) pores. They found out that thiol groups stabilize the AuNPs firmly into particular pores, maintaining their nucleation, and keep them apart. During the synthesis, AuNPs were completely reduced from Au(III) to Au(0) in the methanol solution, a fact that was confirmed by XPS analysis and the presence of the peak at 550 nm in the UV-vis spectrum due to the LSPR effect of AuNPs [70].

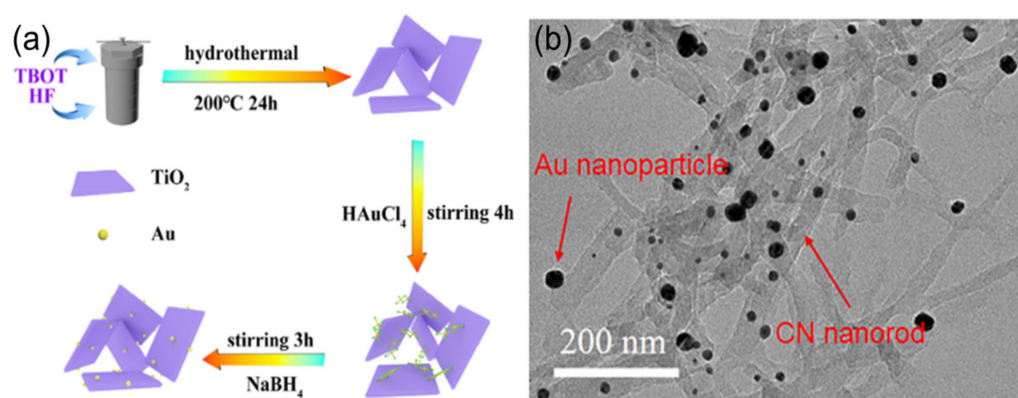


Figure 2. (a) Schematic representation of the fabrication of Au/TiO₂ (Reprinted from [64] with permission of Elsevier, 2019) and (b) TEM image of 1%Au-CN nanorods (Reprinted from [66] with permission of Elsevier, 2018).

Silver nanoparticles deposited on different supports have demonstrated their potential in photocatalysis for more than three decades. A study by Stucchi et al. reported the preparation of Ag/TiO₂ by an ultrasound-irradiation-assisted reduction method with high photocatalytic activity in acetone degradation. AgNO₃ salt was used as the silver precursor and NaBH₄ as the reducing agent. Their findings showed an effect from ultrasound treatment on the silver nanoparticles morphology. The ultrasound treatment favors the agglomeration of AgNPs on the TiO₂ surface. Thus, not well distributed and different sizes of AgNPs (between 1 and 10 nm) were obtained. XPS analysis showed the formation of different species of Ag, such as metallic Ag⁰ and Ag₂O [71]. Rabhi et al. doped TiO₂ with Ag using the sol-gel method as a photocatalyst in pharmaceutical effluent degradation. XRD results showed the formation of a tetragonal anatase-rutile phase and the Ag metallic phase. They noticed that increasing the concentration of Ag promotes the increasing of the rutile phase amount in the material [72]. Recently, a low-cost modified combustion method for synthesizing Ag/TiO₂ was reported by Cruz et al. They obtained a tetragonal rutile phase decorated with metallic AgNPs. TiO₂ with a granular morphology was obtained with a size ranging from 0.1 μm to 1 μm, as well as Ag with a size between 0.294 μm to 0.506 μm. The morphology of the obtained materials did not change after use in the photocatalytic degradation of methylene blue [73]. The deposition of AgNPs onto the g-C₃N₄ were also reported. Chen et al. synthesized Ag/P-g-C₃N₄ in a 2 step method. In the first step, P-g-C₃N₄ was fabricated by thermal polymerization. Furthermore, the AgNPs were loaded by a photo-deposition route. The presence of (111), (220), and (311) planes show a cubic structure of AgNPs with a diameter size between 5 to 10 nm and non-uniformly distributed [74]. A more complex system was synthesized by Narkbuakaew et al. It included the formation of a heterojunction between g-C₃N₄ and Ag/TiO₂. The composite was obtained by mixing before producing g-C₃N₄ (by hydrothermal method) with a H₂SO₄ solution. Afterwards, Ag/TiO₂ was added to the aforementioned mixture. The slurry was centrifuged and dried at 60 °C. The TiO₂ particles were discovered to be embedded in g-C₃N₄ sheets and Ag nanoparticles on the TiO₂ surface (Figure 3a). This facilitates photogenerated electron transportation, lowering the recombination process and boosting the photocatalytic properties [75]. For increasing the photocatalytic activity of MOF-based hybrid catalysts, loading with AgNPs also was developed recently. Guo et al. fabricated a MIL-101(Cr)-Ag metal-organic framework with application in CO₂ reduction. A chemical reduction of AgNO₃ by NaBH₄ was used for depositing AgNPs on the MOFs surface. They obtained well dispersed nanoparticles with an average size of 8 nm on different sizes of the MOFs support [76]. Another published paper reported the effect of synthesis method and parameters on photocatalytic degradation of organic pollutants by Ag-MOF hybrids. Thus, Hayati et al. used the loading method and sonochemical irradiation in order to synthesize Ag-MOF. Their findings have shown that Ag-MOFs nanostructures obtained by sonochemical irradiation present a small size and less agglomerated nanostructures with the best photocatalytic response [77]. Bimetallic Au-Ag deposited on semiconductors were also reported [78,79]. Yang et al. focused on tailoring the optical properties and synthesis method of Au-Ag/TiO₂ spheres through variation of Ag to Au ratios. They obtained a well-distributed binary of Au-Ag nanoparticles with a diameter size between 5 and 20 nm. Their optical response is shown in Figure 3b. After loading the noble metal Au-Ag nanoparticles, the absorption peak characteristic to TiO₂ suffered a red-shift from 390 nm to ~460 nm. As a result, the ratio of Ag to Au in addition to the size of Ag or Au nanoparticles can be adjusted to influence the surface plasmon resonance absorption [80].

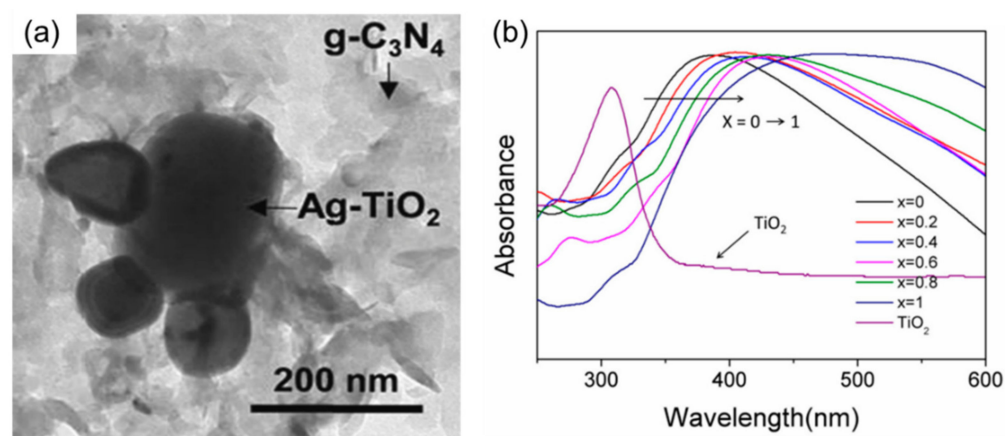


Figure 3. (a) TEM images of Ag/TiO₂/g-C₃N₄ (Reprinted from [75] with permission of Elsevier, 2022) and (b) UV-vis spectra of Au_xAg_(1-x)/TiO₂ composites (x = 0, 0.2, 0.4, 0.6, 0.8, and 1) and the pure TiO₂ spheres (Reprinted from [80] with permission of MDPI, 2020).

3.3. Heterostructures of Non-Noble Plasmonic Metals/Support

In the last few years, non-noble metals (Cu, Ni)-based plasmonic nanoarchitectures have attracted tremendous attention in the field of photocatalysis. Compared to the limited number of counterpart noble metals, the non-noble metals are considerably cheaper, highly available, and offer a broader spectral range of photoactivity, expanding the application area. Regarding the synthesis approaches, the discussion is similar to the many catalysts that require a specific nanoarrangement in terms of particles size, shape, or design (sandwich-like, nanotubes, nanosheets, nanoflakes, etc.) and the bottom-up method is by far preferred to the detriment of the top-down option. Furthermore, the non-noble metals are considerably more prone to form an oxide layer on the surface or even in the bulk regions, which may affect directly the photoresponse. In this regard, and taking into account the already extended focus on the preparation of noble metals plasmon nanoparticles (MeNPs), it is important for the future to draw the level between the advanced noble metal nanoparticles syntheses and, for the moment, primitive non-noble metal plasmons obtaining methods [9,81]. The current section targets the construction methodologies of photocatalysts consisting of non-noble metal nanoparticles (Cu, Ni), coupled with different inorganic or organic semiconductors or supports.

As one of the most studied materials in the photocatalysis field, TiO₂ represents a viable support for plasmonic MeNPs due to its outstanding long-known properties. Wei et al. designed an interesting heterostructure containing Cu NPs deposited on TiO₂ hollow spheres following a series of steps. First, carbon spheres (CS) were decorated with Cu NPs (Cu/CS) via a hydrothermal process. The resulted system was coated with TiO₂ using a controlled hydrolysis approach to obtain the Cu/CS@TiO₂ heterostructure. Finally, the Cu/CS@TiO₂ was calcined to remove the carbon spheres, and the catalyst was photoreduced. The electron microscopy investigations revealed that the resulting material was composed of Cu NPs of around 10 nm and TiO₂ hollow spheres with a diameter between 500–800 nm [82]. A simple and efficient Cu deposition on TiO₂ aerogels was employed by DeSario et al. involving a sol-gel method followed by a classical photodeposition of Cu NPs. Herein, the resulting composite revealed TiO₂ aerogels NPs of 10.3 ± 2.3 nm, while the Cu NPs, consisting of a mixture of Cu⁰, Cu¹⁺, and a very small amount of Cu²⁺, have a relative diameter of 3.2 ± 0.7 nm [83]. Dai et al. built up a photocatalyst consisting of Cu₂O octahedrons decorated with Cu NPs, to form an ohmic junction photocatalyst Cu@Cu₂O. In their study, the synthesis of the Cu₂O octahedrons was the first step, followed by an in situ chemical reduction with Cu⁺. The octahedra-like Cu₂O crystals had diameters between 400 and 800 nm, while the tiny Cu NPs were anchored on the surface of the parental Cu₂O [84].

Recently, Chen et al. assembled a unique doughnut-shaped heterostructure involving TiO_{2-x}/Cu/ZnO. In the first step, a TiO₂/CuO support was obtained in the shape of

doughnut via the spray pyrolysis technique. Next, different thickness layers of ZnO were encapsulated via atomic layer deposition (ALD) on TiO₂/CuO, and the mixture was kept in a reducing atmosphere (Ar/H₂) at 500 °C for 4 h. The size of the doughnut varied in the range of a few μm with small Cu NPs deposited (few nm), while the ZnO layer could be varied due to the versatile method [85]. Organic materials may also be used as active photocatalytic supports coupled with plasmonic Cu NPs, as Xu et al. reported in their study. For the fabrication of the photocatalysts, the authors used a two-step thermal condensation pathway, which resulted in Cu nanocrystals (NCs) (2–5 nm) deposited on g-C₃N₄ nanosheets [86]. Another promising support constructed is represented by MOF materials. The main reasons for their use in the photocatalytic field are directly related to the increased surface area, the ability to accurately tune the porosity network, and their chemical properties. Xiao et al. developed copper-mediated MOF photocatalysts, Cu@UiO-66 and Cu/Cu@UiO-66, as shown in Figure 4a. After following a classical method for the synthesis of UiO-66 MOF material, the authors used two different types of approaches to embed the CuNPs into and onto the MOFs, namely, the double-solvent approach (DSA) and advanced double-solvent approach (ADSA). Electron micrographs showed the formation of UiO-66 octahedrons (approx. 500 nm) and the presence of very small Cu NPs (1–10 nm) only for the samples where Cu loading was considerably increased [87]. Yu et al. focused their work on a very interesting system based on Cu single atoms (SAs) and Au-Cu bimetallic alloy NPs on TiO₂. The preparation procedure followed a step-by-step photoreduction deposition approach and resulted in a nanoarchitecture (Figure 4b) with AuNPs larger than 8 nm deposited on TiO₂ (Au/TiO₂) and a reduced number of Cu clusters (Cu/TiO₂), due to the fact that more Cu is present in the Cu-Au alloy forming Cu_{0.8}Au_{0.2}/TiO₂ [88]. Another attractive and efficient bimetallic alloy of Cu-Ag was integrated in a SiO₂@S-doped graphitic carbon nitride (SC) core-shell design by Babu and collaborators. The obtained pathway involved a chain of syntheses, starting with the SiO₂NPs, followed by the SiO₂@AgCu nanoalloy, and concluding with the core-shell arrangement of SiO₂@AgCu@S-doped C₃N₄. Regarding the morphology of the final material, SiO₂ particles of approx. 120 nm and layers of SC with a thickness between 3 to 5 nm were observed, while the Ag-Cu nanoalloy NPs diameter was determined to be around 1.3 nm [89].

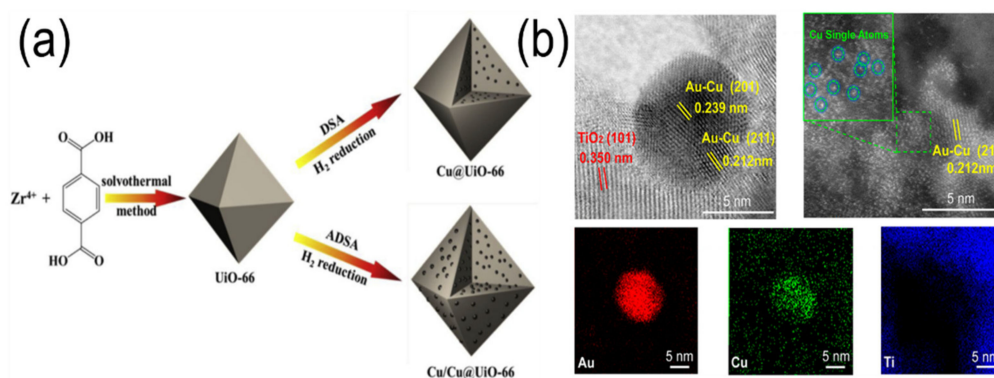


Figure 4. (a) Graphical representation of the Cu@UiO-66 and Cu/Cu@UiO-66 via DSA and ADSA syntheses (Reprinted from [87] with permission of Elsevier, 2019) and (b) HAADF-STEM images (up) and elemental mapping images of Cu_{0.8}Au_{0.2}/TiO₂ (bottom) (Reprinted from [88] with permission of ACS, 2021).

In addition to Cu plasmonic NPs, remarkable results in environmental photocatalysis were observed also in the presence of Ni plasmons containing catalysts. As such, He et al. created a Ni-TiO₂ heterostructure following an adapted mediated nanosphere lithography method. The results showed a homogeneous layer of 200 nm TiO₂ deposited on silica nanospheres, on top of which another layer of 100 nm of Ni was attached. The size of the Ni-TiO₂ top layers with the SiO₂ nanosphere as a core can be tuned specifically to influence directly the optical properties [90]. Wang et al. developed a system consisting of

black TiO₂ nanowire arrays, on top of which size-controlled NiNPs were deposited. The black TiO₂ was obtained via a hydrothermal approach, followed by the thermal hydrogen treatment, while the NiNPs were deposited via atomic layer deposition (ALD). Black titania nanowires characteristics were found to be around 25 nm in diameter and approximately 3.2 μm length. At the same time, NiNPs size could be controlled from the cycles of the ALD applied [91]. Tudu et al. designed another type of heterostructure consisting of a non-noble-metals bimetallic alloy, Cu-Ni, integrated in a TiO₂ thin film. The Cu-Ni alloy synthesis followed a classical hydrothermal approach, using hydrazine hydrate and NaOH solution as a reducing agent and alkali environment, respectively. In order to obtain the Cu-Ni/TiO₂ nanohybrid, the authors used a simple impregnation pathway by suspending the well-known P25 (TiO₂) in ethanol and mixing it with the Cu-Ni alloy suspension in ethanol. The textural investigations revealed the formation of an alloy-semiconductor heterojunction between spherical Cu-Ni NPs with a homogeneous particle size distribution (20–30 nm) and irregular TiO₂ crystals [92]. Kumar et al. had a similar idea to employ the synergistic effect of Cu and Ni in Cu-Ni alloy NPs dispersed in the same P25 (TiO₂) matrix. The synthesis procedure was reported to involve the co-impregnation of TiO₂ with Cu and Ni nitrates, with the formation of the Cu-Ni alloy during the photocatalytic tests as a result of the mild photoreduction conditions. The electron microscopy analysis revealed the intimate contact between Cu-Ni alloy NPs a few nm in size and irregularly shaped anatase/rutile nanocrystals [93].

4. Hybrid Plasmonics in Metal Nanoparticles/Layered Double Hydroxides Heterostructures

By virtue of the excellent adsorption capacity, tunable acidity–basicity [94] and the highly hydroxylated surface, the rigid and crystalline LDH sheets play multifarious roles in heterostructuring PNP/LDH, including immobilization and stabilization of PNPs [95] while providing a unique interface-space confined in a 2-D porous matrix for controlling NPs spatial distribution [96]. On the other hand, serving as a support, the LDH matrix guarantees to stabilize low nuclearity nanospecies on its surface by minimizing atom diffusion, controlling the nanoparticle morphology, and modifying active nanometal electronic structure [97]. As previously mentioned, compared with the single component PNPs/LDHs, heterostructures show the advantages of the synergistic behavior of the coupled nano-units to effectively harvest light during catalytic processes. In this section, we will cover the basics and highlight some relevant studies that we believe illustrate the concept and possibilities of MeNP/LDHs as hybrid nanostructures from the viewpoint of the rational design and the synthesis strategies that will significantly determine their properties in plasmonic catalysis.

4.1. Heterostructures of Noble Plasmonic Metals/ Layered Double Hydroxides

Among a variety of noble metals, the research on heterogeneous catalysis based on AuNPs is one of the most relevant in the literature [98]. Firstly, Zhang et al. achieved the direct synthesis of AuNPs on MgAl-LDH with a homogeneous deposition–precipitation technique using urea as the precipitating agent [99] and HAuCl₄ as the gold precursor. They revealed that very small AuNPs (average size of 2–3 nm) were formed preferentially on the lateral (1010) faces of the LDH nanoplatelets. Varade and Haraguchi further reported a protocol regarding the synthesis of AuNPs/MgAl-LDH by exploiting the exfoliation of stacked LDH layers to provide positively charged nanosheets and further acting as a reducing agent of the NaAuCl₄ precursor [100]. Additionally, several recent publications reported AuNPs/LDH as active heterogeneous catalysts for various catalytic processes, such as: the synthesis of lactones from diols [101], the aerobic oxidation of alcohols under mild reaction conditions [102,103], coupling of nitroarenes to synthesize aromatic azo compounds [103], aqueous oxidation of 5-hydroxymethylfurfural into 2,5-furandicarboxylic acid under atmospheric oxygen [104], or deoxygenation of epoxides to alkenes using molecular hydrogen [105]. Although the aforementioned works reveal interesting applications

in industrial catalysis, the amount of literature on the applications of AuNPs/LDH in plasmonic catalysis is very limited. Carja et al. reported a green preparation of AuNPs/Zn-based LDH and tested their applications as plasmonic catalysts in hydrogen generation by water splitting under irradiation by solar light [12]. It is a green synthesis strategy in which AuNP/LDH is heterostructurally designed by exploiting the manifestation of the LDH “structural memory” property in an AuCl₃ aqueous solution, at room temperature. Notably, AuNPs were obtained directly on the surface of the LDH without using any additional chemical compound. During the clay reconstruction process, Cl[−] were taken by the LDH from AuCl₃ aqueous solution to reconstruct its interlayers, while Au³⁺ were adsorbed organized as nanoparticles on the LDH surface [12]. By varying the LDH composition, noticeable effects from MSI for altering the plasmonic properties of AuNP/Zn-based LDH were noticed. Thus, UV-Vis and XPS results revealed that AuNPs oxidized faster for ZnCeLDH than for ZnAlLDH, leading to a larger steady-state population of positive Au⁺ or Au³⁺ and extended synergy between AuNPs and the LDH. This is important because it shows the impact of the LDH composition on harvesting the characteristics of plasmonic energy so as to modulate the manifestation of PICS in the indirect plasmonic catalysis. Next, some of us presented a detailed investigation on the oxidation state of AuNPs (as Au⁰, Au³⁺, as well as mixed Au⁰/Au³⁺) and their SPR characteristics in AuNPs/ZnAlLDH hybrids by comparing the above-described calcination/reconstruction method and the impregnation/adsorption method [43]. First, we found that the synthesis procedure established both the nanomorphology and the characteristics of the plasmonic response in the designed heterostructures. Both syntheses have given rise to heterostructures where AuNPs smaller than 10 nm are highly dispersed on the larger nanoparticles of ZnAlLDH, with an average size of 110 nm, though the concentration of AuNPs on the large nanoparticles of ZnAlLDH increased when heterostructuring was realized by the calcination/reconstruction method (see Figure 5a–e). The UV-VIS results (Figure 5f), pointing to the red shift of the SPR peak from 539 nm to 547 nm, suggested the quantum size effect of AuNPs led to a lower-energy plasmonic near-field when AuNPs grew during the LDH reconstruction under UV-visible irradiation.

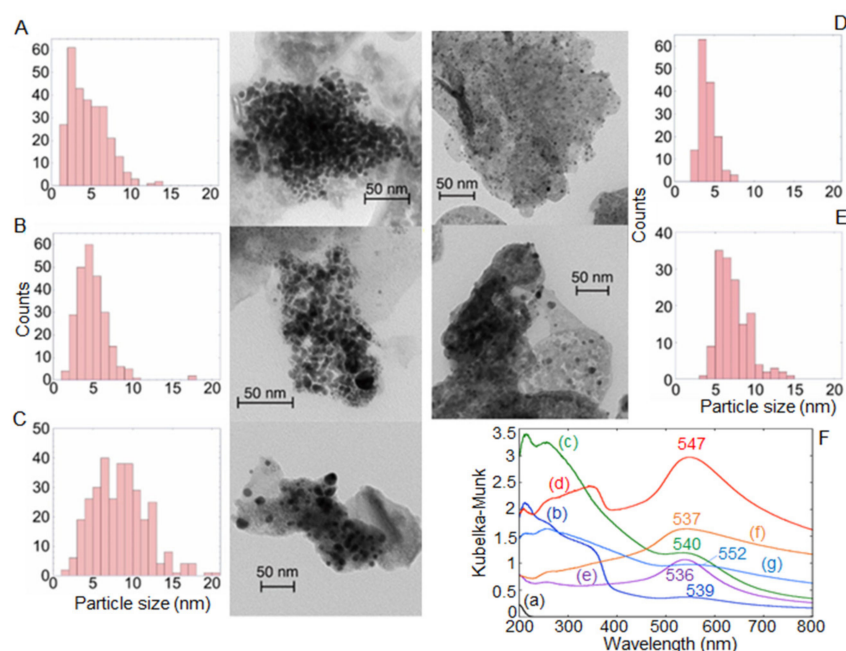


Figure 5. TEM images and analysis for (A) Au/Zn₂Al-Rec-1, (B) Au/Zn₂Al-Rec-2, (C) Au/Zn₂Al-Rec-3-Light, (D) Au/Zn₂Al-Imp-NaBH₄, (E) Au/Zn₂Al-Imp-Lysine and (F) UV-vis absorption profiles of (a) Zn₂Al-LDH, (b) Au/Zn₂Al-Rec-1, (c) Au/Zn₂Al-Rec-2, (d) Au/Zn₂Al-Rec-3-Light, (e) Au/Zn₂Al-Imp-NaBH₄, (f) Au/Zn₂Al-Imp-Lysine, and (g) Au/Zn₂Al-Light (Reprinted from [43] with permission of Elsevier, 2016).

We hypothesized that the special environment in which ZnAILDH, reconstructed by the transformation of the mixed oxides, established tuned MSI that strongly impacted the plasmonic behavior of AuNPs/ZnAILDH. Finally, EXAFS results provided further evidence for the synergistic behavior between AuNPs and ZnAILDH. From this work it is clear that the electron transfer at the interface was faster when the conjunction between nanogold and ZnAILDH was achieved by the calcination/reconstruction method when compared to the impregnation method. Thus, it is revealed that the synthesis procedure can be used, to a large extent, to establish the MSI and the plasmon induced electron transfer characteristics [106]. Another important example is the work of Zhu's research group, which revealed how the incorporation of phosphate anions (PO_4^{3-}) and metal cations (such as Ga^{3+} , Fe^{3+} , and Zn^{2+}) in MgAILDH established characteristics of AuNPs/MgAILDH during the plasmonic catalysis for the reduction of nitroaromatics to azoxy-compounds under visible light irradiation [107]. The detailed procedure describing how MgAILDH was first intercalated with PO_4^{3-} in the interlayers by the reconstruction method and after the junction between AuNPs and PO_4^{3-} /MgAILDH was obtained by impregnation-reduction is shown in Figure 6. The authors claimed that the presence of PO_4^{3-} increased the charge redistribution and internal electric field inside the MgAILDH and facilitated the electron transfer in the designed heterostructure. Furthermore, the introduction of Ga^{3+} , Fe^{3+} , and Zn^{2+} in LDH positive layers resulted in a modified plasmonic response and increased catalytic performances.

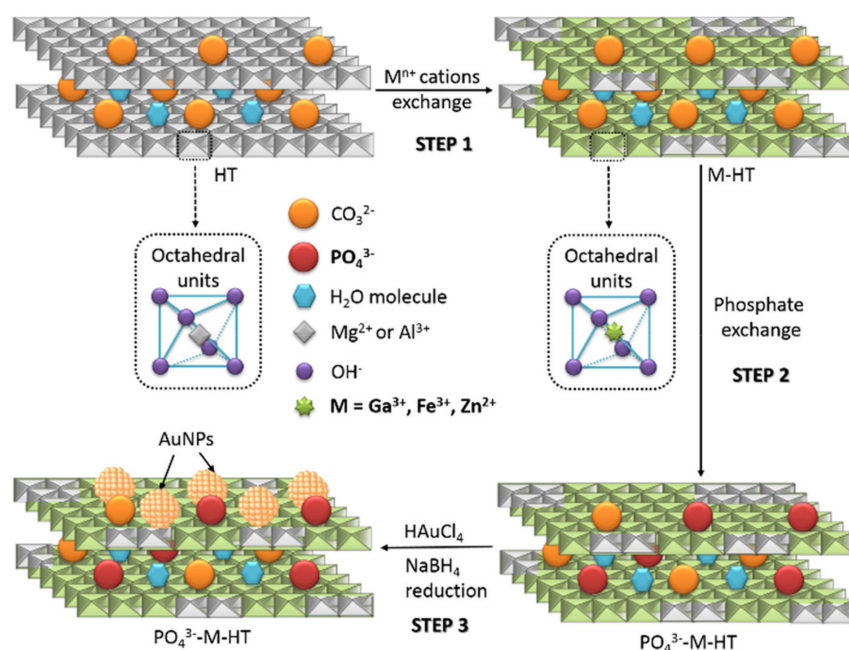


Figure 6. Schematic representation of the synthesis of Au/PO₄³⁻-M-HT catalysts (Reprinted from [107] with permission of Elsevier, 2017).

Similar to our findings, this validates that the LDH composition strongly impacts the plasmonic behavior in AuNPs/LDH and allows for performing chemical reactions beyond those for which only AuNPs play the role of catalytically active sites. Thus, this study revealed the entangled manifestation of a nanoantenna effect [20] by AuNPs and a co-catalytic effect by the substituted MgAILDH in the plasmonic catalysis. Another interesting example in terms of the plasmonic hybridization of AuNPs/LDH was recently reported by Fu et al. [42] by studying visible light promoted degradation of gaseous volatile organic compounds catalyzed on AuNPs/ZnCrLDH. The catalysts were obtained in an aqueous medium containing ZnCrLDH, HAuCl₄ for gold precursor, and NaBH₄ as a reducing agent. AuNPs/ZnCrLDH nanomorphology was defined by almost spherical AuNPs with an average diameter of 8.6 nm well-dispersed on the LDH surface. In particular,

Mott–Schottky measurements (Figure 7a) revealed a synergistic effect between AuNPs and ZnCrLDH, which could result in a major change of the band position compared to the bare LDH. Electrochemical impedance spectra (EIS) and Nyquist plots of ZnCrLDH and AuNPs/ZnCrLDH electrodes (Figure 7b) point out a suppression of the charge recombination generated by PICS. Furthermore, the absorbance at 680 nm vs. time for the open-circuited ZnCrLDH film electrode and AuNPs/ZnCrLDH in a N_2 -saturated acetonitrile ethylene glycol solution under visible light illumination before and after O_2 bubbling (Figure 7c) demonstrated the easier transfer of photoexcited electrons from ZnCrLDH to AuNPs due to the combined LSPR effect after coupling. Moreover, by monitoring the spectrum changes for the AuNPs/ZnCrLDH in the N_2 -saturated electrolyte without donor, before and after O_2 bubbled, under visible light irradiation (Figure 7d), it was found that AuNPs accepted electrons from ZnCrLDH. A dual electron transfer from AuNPs to ZnCrLDH and the opposite transfer from ZnCrLDH to AuNPs should be noticed. Notably, this allows for the conceptualization of new designs of plasmonic heterostructures able to manifest both PICS and co-catalytic effects, thus, to favor the competition between direct and indirect plasmonic catalysis [108].

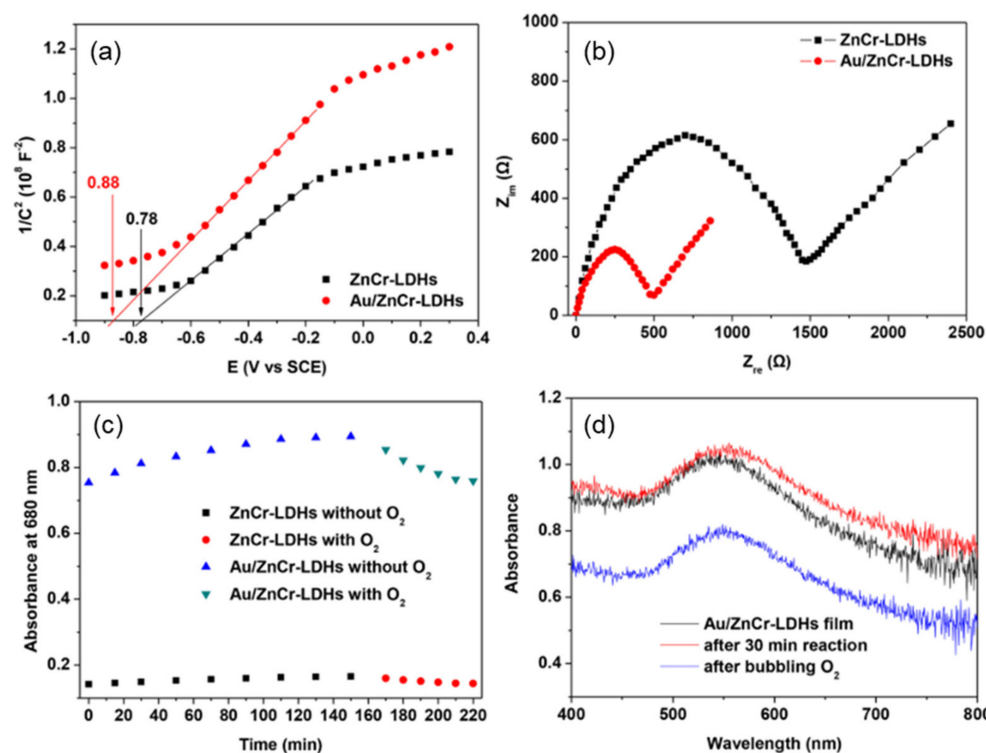


Figure 7. (a) Mott–Schottky (MS) graphs and (b) electrochemical impedance spectra (EIS) Nyquist graphs of ZnCr–LDHs and Au/ZnCr–LDHs electrodes; differences in absorbance at 680 nm for the open-circuited ZnCr–LDHs and Au/ZnCr–LDHs films under exposure to visible light irradiation (c) prior and (d) after O_2 bubbling in a N_2 -saturated acetonitrile ethylene glycol mixture prepared by adding 0.1 mol/L $LiNO_3$ and 0.5 mol/L ethanol. Note: the EIS experiments were carried out with a redox sample of 0.50 mol/L Na_2SO_4 and 2.5 mmol/L $K_3[Fe(CN)_6]/K_4[Fe(CN)_6]$ aqueous solution (Reprinted from [42] with permission of Elsevier, 2019).

There were a number of recent reports concerning AgNPs/LDH heterostructures obtained by diverse synthetic strategies, including precipitation/thermal decomposition [38], anion-exchange precipitation method [109], and photoreduction [110] to obtain AgNPs/LDH heterostructures for catalysis. A good example is the work by Tonda and Jo, that describes Ag/NiAlLDH/g- C_3N_4 composite for the efficient visible-light-driven photocatalytic removal of organic pollutants. The strategy to obtain Ag/NiAlLDH/g- C_3N_4 composite was an in situ hydrothermal method, followed by photoreduction. In brief,

LDH/CN composites were obtained by an in situ hydrothermal process. Thereafter, a series of Ag/NiLDH/C₃N₄ with 1 wt% Ag and 5, 10, 15, and 20 wt% LDH to C₃N₄ were obtained through the adsorption of AgNPs and their subsequent photoreduction using methanol as a hole [110]. The results of the transient photocurrent (Figure 8a) and electrochemical impedance spectroscopy (EIS) measurements (Figure 8b) validated the transfer of photogenerated charge carriers within the nanocomposite system and the charge carrier separation efficiency. By taking advantage of better transfer efficiency of photoinduced charge carriers AgNPs/LDH/CN achieved a more effective charge separation compared to Ag/CN and LDH/CN. UV-vis analysis (Figure 8c) pointed out that the presence of AgNPs improved the light absorption over the whole wavelength regions and the intensity of the plasmonic response is a function of the silver content. Additionally, the junction between AgNPs and LDH/CN strongly decreased the intensity of photoluminescence (PL) spectra, as indicated in Figure 8d, revealing a mixing of the electronic states of the coupled components able to generate strong MSI characteristics between the plasmonic AgNPs and NiALDH/CN. This impacted both the electron–hole separation and the transfer of photogenerated charge carriers [111] between the three-component heterojunction system and established a lower recombination probability for photoinduced electrons and holes. Furthermore, a synergistic response in AgNPs/LDH was reported by Gilea et al. [37]. Specifically, we described AgNP/ZnALDH and AgNP/MgALDH as nanostructured assemblies that were synthesized in an aqueous solution, at room temperature, by exploiting the structural reconstruction of the calcined ZnALDH/MgALDH in the solution of Ag₂SO₄. The SPR features were effective to promote the behavior of AgNPs as both the light harvesting unit and the catalytic component for the process of phenol photodegradation from aqueous solutions, as shown in the next section. Lestari et al. [36] reported the synthesis of AgNPs/ZnALDH by the intercalation of AgNPs in the interlayer space of LDH exfoliated by dodecyl sulfate anions. Similarly, the excellent activity for phenol photodegradation in the aqueous solution was attributed to the manifestation of PICS during the electron donation from the plasmon-excited AgNPs to the conduction band of the ZnALDH semiconductor. The choice to combine the multiplasmonic response arising from different metallic plasmonic nanoparticles, via LSPR, might enable expansion of nanoplasmonics from the visible and near-infrared range toward the ultraviolet range. Thus, support tuning strategies to synthesize multiplasmonic catalysts are strongly required for the ultimate performance in hybrid catalysis. Recently, we studied in detail the plasmonic responses of PtNPs/LDH and PtNPs-AgNPs/LDHs heterostructures, obtained by the calcination reconstruction strategy, for the photocatalytic degradation of p-nitrophenol [40]. The role of the chemical composition of the LDH, as that partially defines the starting point for MSI, was analyzed by following the partial substitution of Zn²⁺ by Fe²⁺ in the composition of the PtNPs-AgNPs/LDH. The significant increase in the photoluminescence signal for Pt-AgNPs/ZnFeAl, as compared to Pt-AgNPs/ZnAl, indicated a retard recombination of electrons–holes in Pt-AgNPs/ZnAl and further validated the active role of the LDH composition to establish an effective electronic coupling and to inhibit the recombination of photogenerated charge carriers. In terms of light absorption properties, multiplasmonic Pt-AgNPs resulted in an extended SPR response in the visible and infrared regimes of the electromagnetic spectrum and improved the caption of the photogenerated electrons, unfolding the reasons for the superior catalytic activity. Similarly, Sahoo et al. reported that the multiplasmonic response of the AuNPs-PdNPs/ZnCrLDH/MCM-41 heterostructure was different from those of single AuNPs and PdNPs [112].

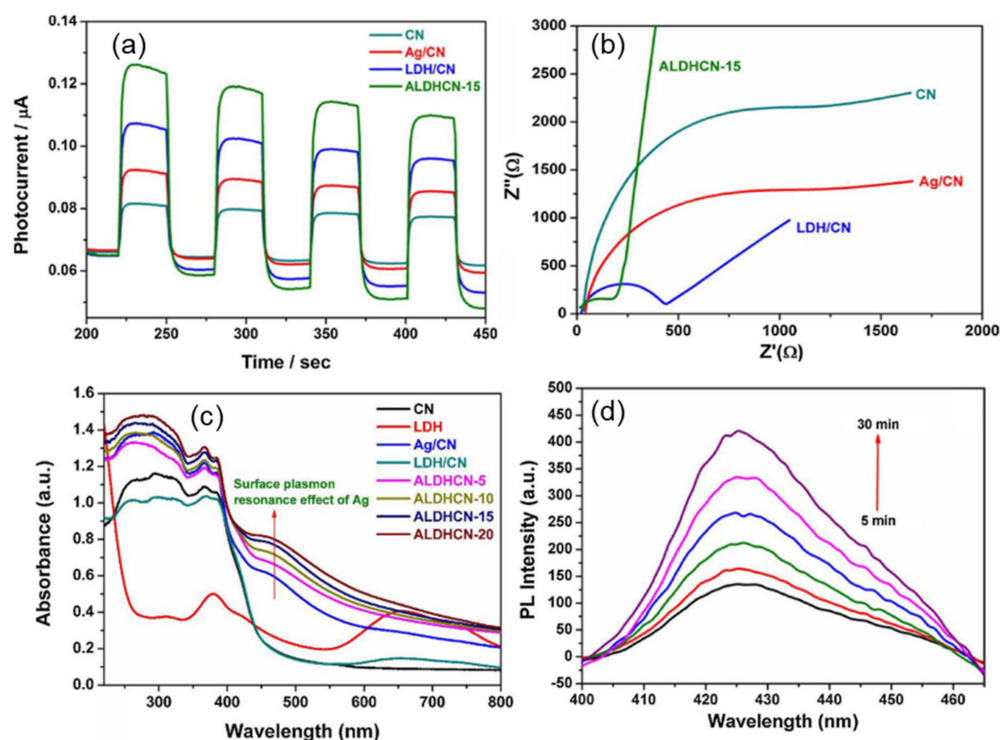


Figure 8. (a) Plots of photocurrent responses, (b) EIS curves of CN, Ag/CN, LDH/CN, and ALDH-CN-15 photocatalysts, (c) UV-vis-DR profiles of CN, LDH, Ag/CN, LDH/CN, and Ag/LDH/CN catalysts and (d) $\cdot\text{OH}$ capturing PL profiles of ALDH-CN-15 in TA solution under visible-light illumination (Reprinted from [110] with permission of Elsevier, 2018).

Table 1 presents the photocatalytic applications of noble metals/LDH heterostructures.

Table 1. Plasmonic noble metals/LDH heterostructures for photocatalytic processes.

LDH	PNPs	Photocatalytic Application	Reference
ZnAILDH and ZnCeAILDH	Au	H ₂ production from by water splitting	[12]
ZnCrLDH	Au	Degradation of VOCs	[42]
ZnAILDH	Au	Phenol degradation	[43]
MgAILDH	Au	4-nitrophenol degradation	[94,95]
MgAlCr-HT	Au	Aerobic oxidation of alcohols	[98]
MgAILDH	Au	Aqueous oxidation of 5-hydroxymethylfurfural	[99]
MgAILDH	Au	Deoxygenation of epoxides to alkenes	[100]
M-MgAILDH (M = Ga ³⁺ , Fe ³⁺ , Zn ²⁺)	Au	Selective reduction of nitroaromatics to azoxy-compounds	[102]
ZnAILDH	Ag/Ag ₂ O	Tetracycline degradation	[38]
NiAILDH/CN	Ag	RhB and 4-CP degradation	[105]
ZnAILDH and MgAILDH	Ag	Phenol degradation	[37]
ZnAILDH	Ag	Phenol degradation	[36]
ZnTiLDH	Ag	Degradation of Rhodamine-B (RhB) and NO _x	[41]
ZnAILDH and ZnFeAILDH	Pt, Pt-Ag	p-nitrophenol degradation	[40]
ZnCr LDH-MCM-41	Pd, Au-Pd	One pot synthesis of imines	[107]

4.2. Heterostructures of Non-Noble Plasmonic Metals/Layered Double Hydroxides

While extensive reports exist on plasmonic catalysts based on noble metals nanoparticles, information about non-noble metals PNPs/LDH nanostructures remains scarce [81]. However, compared to noble-metal based plasmonic NPs the non-noble analogues are less expensive and might exhibit comparable performances to convert light energy by heterogeneous catalysis [113]. However, to date, few studies exist regarding the plasmonic properties of heterostructures of non-noble plasmonic metals/layered double hydroxides and their applications. CuNPs are just starting to be explored in plasmonic catalysis [61]. To obtain CuNPs/LDH heterostructures, Ma et al. reported a reduction procedure by using MgCuAILDH and ascorbic acid for the reduction of copper [114]. By taking advantage of the tuned copper content of MgCuAILDH, they obtained a broad size range of Cu₂O nanoparticles highly dispersed on MgAILDH. Furthermore, XRD, TEM, and XPS results disclosed a close conjunction of Cu₂O nanoparticles with MgAILDH that promoted their photocatalytic behavior under visible light while degrading orange II from water. To investigate the plasmonic optical responses in CuNPs/LDH heterostructures, some of us obtained CuNPs/ZnAILDH and CuNPs/MgAILDH heterostructures as active photocatalysts for the degradation of the industrial dye Nylosan Navy (Clariant Produkte) by irradiation of both Vis and UV light [115]. CuNPs/LDH nanoarchitectonics were synthesized by a simple and cost effective method based on the formation of nanoparticles of CuO on the surface of the eco-friendly clay during the structural reconstruction of the layered LDHs matrix in the aqueous solution of Cu(OAc)₂. The derived solid solutions were obtained by calcination of CuNP/LDH at 750 °C. Investigations into the optical properties demonstrated a synergistic response between CuNPs and the LDH, while results from the optical direct band gap (E_g) values of the samples revealed narrow band gap values (3.34 eV for Cu/MgLDH, 3.21 eV for Cu/ZnLDH that decreased to 2.1 and 1.47 eV after the calcination). This is likely to promote plasmonic capabilities and disclose the semiconductor characteristics, while the electron transfer across the dye-semiconductor interface was found to increase the charge carrier lifetime and evidence the co-catalytic effect. To combine multiplasmonic responses for mitigating the limited visible light absorption in catalysis, the fabrication of Au-CuNPs/MgAILDH catalysts was achieved by the impregnation-reduction method, by using HAuCl₄ and Cu(NO₃)₂ as precursors and NaBH₄ as a reduction agent [116]. Importantly, the resulting Au-CuNPs/MgAILDH showed better performances in the oxidative esterification of benzyl alcohol with methanol in the presence of molecular oxygen to prepare methyl benzoate under visible-light irradiation in comparison to single plasmonic components, AuNPs/MgAILDH and CuNPs/MgAILDH, respectively. XPS results disclosed that the junction between Au with Cu led to electrons preferentially transferring from Au to Cu and facilitated the successful reduction of the oxidized surface Cu. Although the impact of MgAILDH composition in the catalytic process is clearly demonstrated, the extent to which the electrons are transferred between the LDH and the plasmonic NPs by manifesting PICS and/or co-catalytic effect is not studied in this work.

The construction of NiNPs/LDH heterostructures was further explored as an effective means for obtaining an extended response in plasmonic catalysis. Plasmonic NiNPs display a localized yet tunable SPR in the UV–vis–NIR regions and offer the perspective in synthesizing highly active catalysts [117], although the exploitation of their plasmonic features still remains a pressing challenge and the amount of literature on the synthesis of NiNPs/LDH heterostructures is limited. Carja et al. developed heterostructures of NiNPs/MgAILDH and NiNPs/MgFeLDH by a calcination-reconstruction method [118]. In an aqueous medium, at room temperature, NiNPs within the size range up to ca. 10 nm were highly dispersed on the surface of MgAILDH and MgFeLDH by the mediated reconstruction in NiSO₄·7H₂O solution. The SPR response of NiNPs is synergistically combined with the optical features of the LDH support. In 2021, Li et al. reported highly dispersed metallic NiNPs/NiAILDH [119]. The specificity of the preparation method was assigned to the formation of NiNPs through the rationally designed mild liquid reduction method, described in Figure 9a. The XRD (Figure 9b) and HRTEM results clearly indicated

the structural characteristics of the joined NiNPs and NiAlLDH nanounits with the NiNPs average size of ~10 nm. Ni/NiAlLDH, obtained after 12 h reductions, exhibited obvious absorption across the entire solar spectrum (220–2000 nm) due to the surface plasmon absorption of metallic Ni. As revealed in Figure 9c, UV–vis-IR absorption results showed a wide SPR response defined by the absorption band at 645–710 nm due to the $3A_{2g}(F)3T_{1g}(F)$ transition, attributed to the spin–orbit coupling of nanosized Ni [120]. As a result, the plasmonic enhancement for Ni/NiAlLDH was strongly enhanced when compared to NiAlLDH for the wavelength range higher than 500 nm.

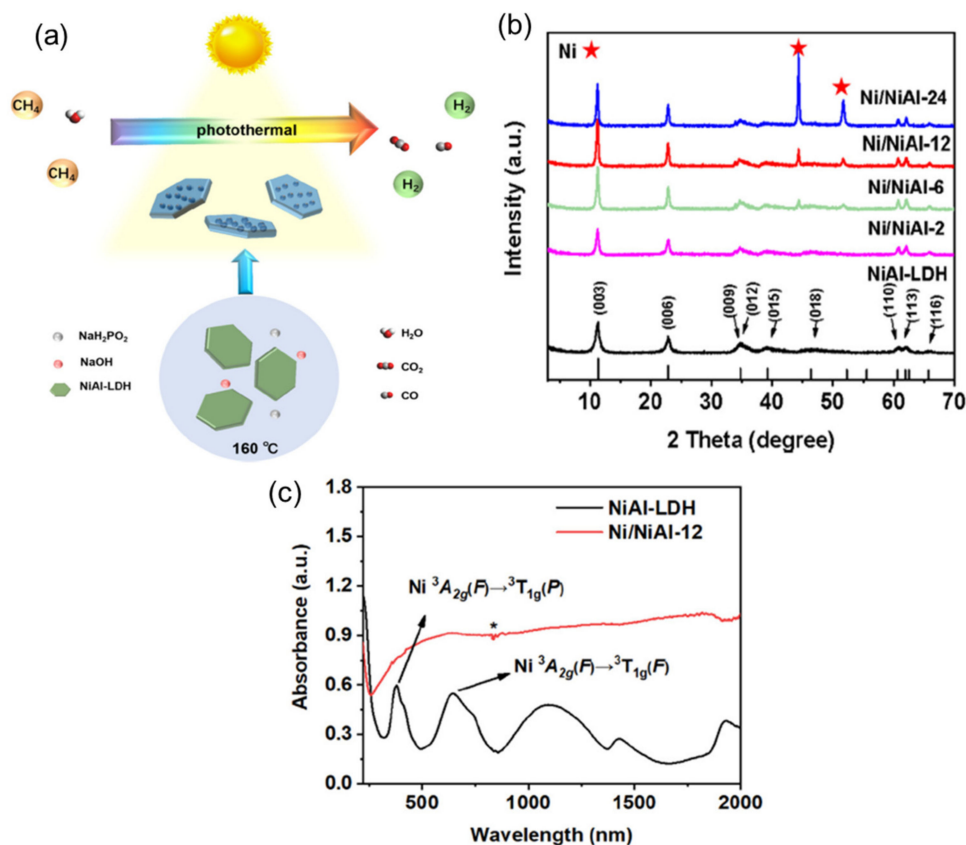


Figure 9. (a) Schematic illustration of the synthesis of Ni/NiAl-*x* for H₂ generation from CH₄ and H₂O under solar light irradiation (b) XRD spectra of the samples produced under various reduction times and (c) UV–vis-IR absorption profiles of the obtained materials (The jump point marked by * is assigned to the instrument light) (Reprinted from [119] with permission of Elsevier, 2021).

5. Metals/Layered Double Hydroxides Heterostructures for Applications in Plasmonic Catalysis

Mikami et al. reported the degradation of a toxic organic compound (phenol) from an aqueous solution by Au/ZnLDHs under solar light irradiation synthesized by the reconstruction and impregnation method. The parent LDH showed 7.6% of phenol degradation, while after gold deposition, the efficiency of the photocatalysts reached complete decomposition. The best catalyst was found to be reconstructed under solar light irradiation (Au/Zn₂Al-Rec-3-Light). Samples synthesized by the reconstruction method showed a better photocatalytic activity compared with the one obtained by the impregnation method. As well, two different degradation pathways were noticed. An indirect ring opening process (through the formation of p-benzoquinone) describes the degradation by reconstructed materials and both indirect and direct opening ring processes (through the formation of catechol, o-benzoquinone, and then muconic acid) by impregnated materials. A key role in the photodegradation process had the oxidation state of gold nanoparticles (Au⁰, Au³⁺, and mixture Au⁰/Au³⁺) deposited on the layered double hydroxide surface. Therefore, in order

to achieve O_2 reduction, the fast electron transfer from LDH to Au sites was influenced by the interface of the Au_2O_3 phase between metallic Au^0 and LDH. Since Au^0 NPs were not very well incorporated into the impregnated sample surface, it caused a slower electron transfer at the interface and a reduced charge separation efficiency. This study also revealed that increasing the Au nanoparticle's dimension and SPR intensity had no effect on the photocatalytic efficiency. Furthermore, a correlation between the surface of the catalyst and efficiency could not be found. The best catalyst (Au/Zn₂Al-Rec-3-Light) proved to have good stability after five cycles of reusing. A minor decrease in efficiency of 30% was noticed. An approximately 10% increase in photocatalytic activity was observed after irradiation of the recovered catalyst after reuse. This can be explained by charge transfers between AuNPs and LDH produced under irradiation [43].

AuNPs/LDH showed good performance in the photocatalytic water splitting process. A study by Carja et al. reported Au/ZnAlLDH and Au/ZnCeAlLDH with high H_2 production from water splitting. They underlined the impact of the LDH composition and AuNPs dimension in photocatalytic H_2 generation. Thus, by adding Ce into the LDH composition the hydrogen production increased even though almost the same amount of gold was deposited on ZnAlLDH and ZnCeAlLDH. Calcined samples exhibited lower photocatalytic efficiency due to an increase in the size of AuNPs, causing a weak interaction between the metal nanoparticles with the support (SMSI). Another important factor is the distribution of the metallic (A^0) and cationic gold ($+$ and $^{3+}$) on the surface. Since the Au NPs introduce electrons into the LDH's conduction band, there ought to be an abundance of positive charge-density Au atoms. The presence of Ce from the LDH matrix promotes the electron injection, which increases the steady-state population of positive Au ($+$ or $^{3+}$) atoms in the material. Therefore, the deposited gold is oxidized more quickly throughout the photocatalytic process [12].

Xiao et al. investigated the reduction of nitroaromatics (nitrobenzene) to azoxy-compounds (azoxybenzene) by Au/LDH heterostructures under visible light irradiation. They tailored the hydrotalcite (HT) support by adding phosphate (PO_4^{3-}) and metal ions M (such as Ga^{3+} , Fe^{3+} , and Zn^{2+}) in order to prevent the production of azo- and aniline compounds. Compared to the M-HT, PO_4^{3-} -HT, and HT supports, Au/ PO_4^{3-} -M-HT were the most effective photocatalysts, especially Au/ PO_4^{3-} - Ga^{3+} -HT. It showed good selectivity for azoxy compounds and high conversion. Reusing tests of five cycles for the best catalyst without any changes in activity proved good stability in this process. Furthermore, they explored the influence of light irradiation at different wavelength ranges by using block filters. It was noticed that conversion decreased for the wavelengths below 550 nm and 600 nm, while the range of 490–600 nm overlaps with the LSPR of gold nanoparticles, suggesting an antenna effect in AuNPs. The influence of light intensity and temperature of the reaction was also explored. The conversion increased linearly with the increase in temperature and light intensity until $0.7 W/cm^2$; afterward, it increased non-linearly with the light intensity (Figure 10a). In order to obtain a full conversion, it was necessary to increase the temperature to $50\text{ }^\circ C$ and the light intensity to $0.9 W/cm^2$. The electron transfer mechanism from Figure 10b shows the transfer of the light excited electrons into the conduction band of the support in order to create a positive charge density of AuNPs and to start the reaction. Additionally, PO_4^{3-} can also contribute to the electron transfer due to an increase in charge distribution. In conclusion, the reduction of nitrobenzene to nitrosobenzene (step 1) is possibly due to the energy generated by light-excited electrons of gold nanoparticles that activate the N-O bond. Furthermore, nitrosobenzene transforms very fast in phenylhydroxylamine, which can couple with nitrosobenzene and form the azoxy compound [107].

Volatile organic compounds (VOCs) were also removed by the photocatalytic process using heterostructures with AuNPs and LDH. These compounds are very toxic, mutagenic, and carcinogenic. Fu et al. reported the photocatalytic degradation of o-xylene by ZnCrLDH and Au/ZnCrLDH, as well as the influence of some factors, such as catalyst dosage, concentration of the pollutant, the temperature of the reaction, light intensity, and relative humidity. This study pointed to an increase in the photocatalytic efficiency after increasing

the amount of gold deposited on the LDH surface and a decrease in the removal rate after the increase in the concentration of *o*-xylene. Furthermore, a study on the effect of the catalyst dosage, radiation intensity, and temperature of the reaction showed an increase in the removal rate with the increase in these parameters. As in the study carried out by Xiao, photocatalytic tests were carried out at different wavelengths range. In this case, they noticed that between 500–600 nm Au/ZnCrLDH showed the best efficiency due to the LSPR of gold nanoparticles. The photocatalytic mechanism can be described as follows: to avoid the recombination of $e^- - h^+$, gold nanoparticles deposited on the surface can serve as an acceptor of e^- from the LDH support. In this way, holes would receive more opportunities to act individually for gaseous *o*-xylene photodegradation so that more electrons and holes may participate in the production of hydroxyl radicals. Because of this, Au supporting can significantly improve the photocatalytic performance of LDHs [42].

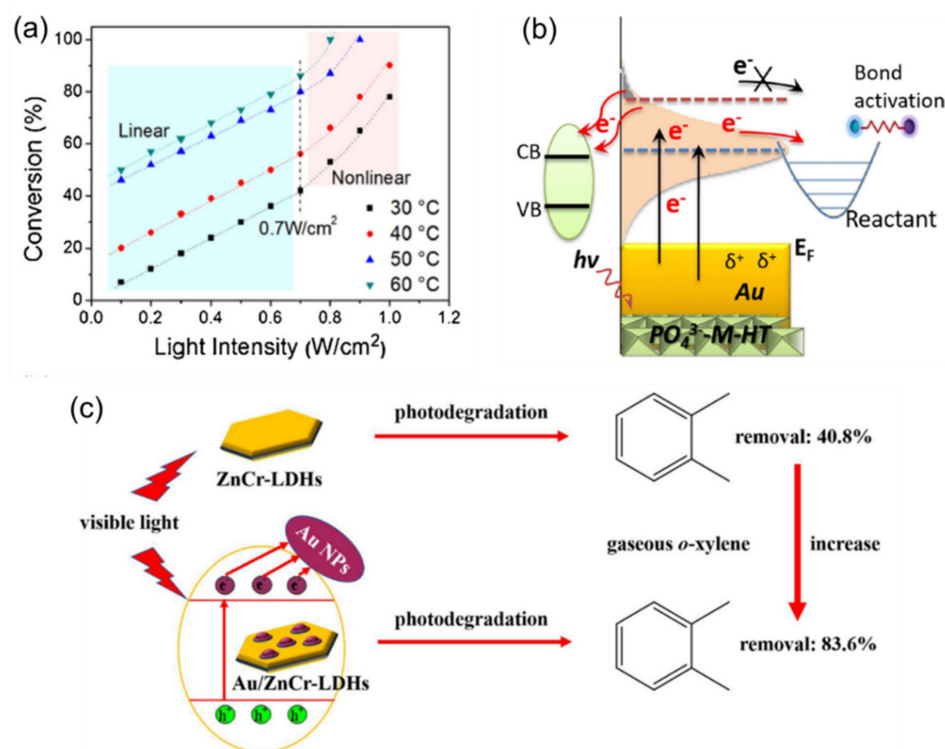


Figure 10. (a) Temperature-dependent photocatalytic efficiency as a function of light intensity, (b) Schematic illustration of the electron transfer mechanism in Au/PO₄³⁻-M-HT under irradiation (Reprinted from [107] with permission of Elsevier, 2017) and (c) Schematic representation of mechanism and photocatalytic efficiency in volatile gaseous compounds removal by Au/ZnCrLDH (Reprinted from [42] with permission of Elsevier, 2019).

Silver decorated layered double hydroxides have also attracted the attention of scientists in past years for use as photocatalysts. Thus, only a few examples will be further discussed. Tonda and Jo studied the photocatalytic efficiency of Ag/LDH/g-C₃N₄ nanocomposites in the degradation of Rhodamine B and 4-chlorophenol. For this study, different amounts of NiAILDH (5, 10, 15, and 20%) were used for the synthesis of LDH/g-C₃N₄ and 1% Ag for the decoration of LDH/g-C₃N₄. The best results in degradation of both RhB and 4-CP were obtained on Ag/LDH/g-C₃N₄ with 15%LDH. This catalyst was recovered and reused in another five photocatalytic cycles (Figure 11a). It showed good stability in this reaction due to the charge transfer among CN and LDH, also the ability of AgNPs to effectively capture electrons. The proposed mechanism shown in Figure 11b shows the migration of the electrons from the CB of CN to CB of LDH excited by solar light irradiation. Furthermore, the charge separation forms due to the displacement of the holes from the band VB of LDH to the VB of CN. AgNPs from the surface act as electron traps and capture the electron from the CB of

LDH and CN. The loaded AgNPs and the interface between the CN and LDH prevent the recombination of the charged carriers. As a next step, electrons from the AgNPs surface reduce dissolved oxygen in $O_2^{\cdot-}$ species, followed by its conversion in $\cdot OH$. The generated $O_2^{\cdot-}$, $\cdot OH$ species combined with photogenerated holes degrades pollutants such as RhB and 4-CP [110]. The photodegradation of antibiotics such as tetracycline (TC) by silver decorated ZnAlLDH (LDH-Ag₂O/Ag) was reported by Chen et al. As shown in Figure 11c, under visible light irradiation, TC did not self-degrade, and pristine LDH showed a low degradation. After the decoration with silver nanoparticles, the photocatalytic performance increased to 65–92% in 90 min. The amount of silver used in the synthesis of the materials played an important role in their performance. It increased with the increasing content of Ag species. A higher amount of Ag species (15%) favors the recombination of e^-h^+ , decreasing the performance of the catalyst. A stability test for the best catalyst after five cycles was performed in this case too, which showed a slight decrease in performance. These results proved good stability and high photocatalytic degradation of TC. Ag₂O on the surface of LDH generates electron–hole pairs as a result of visible light irradiation. The ZnAl LDH, on the other hand, cannot be activated by visible light. Therefore, some photogenerated electrons from CB of Ag₂O can be transferred to CB of ZnAlLDH because of the greater negative CB position. Following that, ZnAlLDH serves as a platform for the reactions to stimulate the formation of dissolved oxygen radicals, which are then converted to OH by interacting with H₂O. The fact that the VB position of Ag₂O is significantly higher than the redox potential of OH/H₂O shows that the holes on the VB Ag₂O cannot oxidize H₂O to $\cdot OH$. Therefore, h^+ on the VB of plasmonic silver would directly interact with TC. However, due to the SPR effect of silver species, additional visible light photons may be absorbed, which would result in a transfer of photoinduced electrons between the silver species. Thus, as one of the active species ($\cdot OH$, h^+ , and $\cdot O_2$), $\cdot OH$ significantly impacted the effective degradation of TC into intermediates and ultimately to CO₂ and H₂O (Figure 11d) [38].

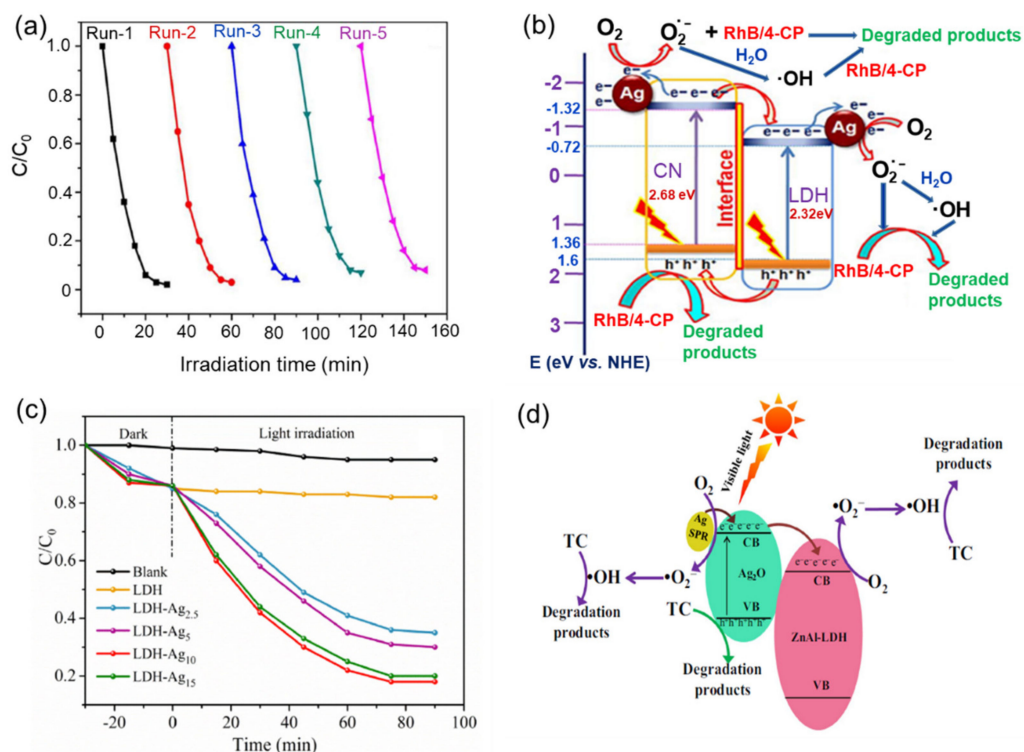


Figure 11. (a) Recycling results of Ag/CN/LDH-15 in photodegradation process of RhB, (b) graphical representation of the mechanism in photodegradation of RhB/4-CP by Ag/CN/LDH (Reprinted from [110] with permission of Elsevier, 2018), (c) Photocatalytic efficiency of pristine LDH and Ag/Ag₂O/LDH in TC degradation and (d) Graphical representation of TC degradation via a potential photocatalytic process by Ag/Ag₂O/LDH (Reprinted from [38] with permission of Elsevier, 2019).

A new study demonstrated the efficiency in the photodegradation of phenol by intercalating Ag between the LDH layers and not by its traditional deposition on the LDH surface. A comparison study was performed with different species intercalated (HCO_3^- , Cl^- , dodecyl sulfate, $\text{Ag}(\text{CN})_2$, and Ag) and P25. The best results were obtained on ZnAlLDH/Ag (80% degradation). In this case, after irradiation, silver nanoparticles acted as an electron source that migrated from the plasmon-excited silver to the conduction band of LDH. The superoxide radicals were created and reduced phenol due to the interaction of the e^- from the conduction band with the e^- acceptors [36].

Bimetallic nanoparticles supported on layered double hydroxides were also reported as good catalysts in the photodegradation of organic pollutants. A study by Darie et al. reported mono-bimetallic plasmonic (Pt/Pt-Ag) nanoparticles deposited on layered double hydroxides (ZnAlLDH and ZnFeAlLDH) as active photocatalysts in the degradation of p-nitrophenol. Their results showed that Pt-AgNPs/ZnAlLDH was more efficient compared to PtNPs/ZnAlLDH, with a 77% degradation under solar light irradiation. While introducing Fe in the LDH structure, the photocatalytic efficiency decreased drastically to 23% degradation for Pt-AgNPs/ZnFeAlLDH, even though the amount of Pt and Ag deposited on both LDHs was the same. In this case, the degradation mechanism had a different pathway. The presence of iron in the LDH structure favors the reformation of p-nitrophenol from the p-nitrophenolate ion, preventing its degradation by forbidding the electron transfer between the LDH and Pt/Pt-Ag nanoparticles. Therefore, so-called tandem photocatalysis is present. Reusing the catalyst in the three photocatalytic runs showed a slight decrease of 10% in the efficiency of the catalyst, implicitly demonstrating its stability in such processes [40]. Sahoo et al. reported the activity of bimetallic Au-Pd loaded on ZnCrLDH-MCM-41 in the synthesis of imines from oxidation and reduction of benzyl alcohol and nitrobenzene under visible light irradiation. Their results proved an increase in the photocatalytic conversion of benzyl alcohol after the deposition of bimetallic Au-Pd compared with the pristine LDH, MCM-41 or LDH-MCM-41, even compared to single metallic Au/LDH-MCM-41 and Pd/LDH-MCM-41, respectively. The same photocatalytic efficiency was obtained for the tandem reaction of imine synthesis from benzyl alcohol and nitrobenzene [112].

Regarding the applications in plasmonic catalysis of non-noble metals PNPs, Wang et al. developed an Au-Cu@LDH photocatalyst able to oxidize the benzyl alcohol and to further form an ester with methanol under visible light irradiation. In their proposed mechanism, the synergistic effect of Au-Cu alloy NPs and the surface chemistry (base-acid sites) of the Mg_3Al -LDH support were mainly responsible for the catalytic reaction. More precisely, the Au-Cu alloy is possibly directly implicated in the cleavage of the C-H bond due to the existence of light-excited electrons that interact with the intermediate molecules. At the same time, the authors suggested that the cleavage of the O-H bond was caused by the interaction of the benzyl alcohol with the basic-acid sites of the MgAl -LDH. The unsaturated metal active sites of the alloy coordinated a benzyl alcohol intermediate due to the LSPR effect and created a metal-H bond in a metal-alcoholate-LDH system. Moreover, the light-excited electrons induced the formation of aldehydes from the metal-alcoholate-LDH while also promoting the formation of $\text{O}_2^{\bullet-}$ radicals, which are further involved in the catalytic process. To conclude here, the Au-Cu plasmons showed multiple roles in this particular photocatalytic reaction [116]. Liu et al. reported a combination of light assisted thermal-driven CO_2 reduction with methane towards syngas (DRM), in the presence of a Ni/ Al_2O_3 catalyst. The suggested photomechanism is based on Au plasmonic features, which the authors extrapolated to expected Ni plasmon properties. As such, the hot electrons light-generated by NiNPs LSPR may be capable of activating the CH_4 and CO_2 molecules at a lower scale than Ag and Au but enhanced by the thermal assistance. Herein, the NiLSPR accelerated the reaction between the already activated species CH_x^\bullet and O^\bullet , and it is believed that the NiLSPR activates preponderantly the CO_2 radicals, which are further desorbed, providing more active sites for the classical thermal activation of CH_4 radicals. In this way and similar to the case of Wang et al. [116], Ni

plasmon show different roles in the ambitious proposed mechanisms [117]. Recently, in a comparable synergetic system involving light and thermal input as Liu et al., Li and co-workers reported remarkable steam methane reforming (SRM) towards H₂ results. As catalyst for the photothermal experiment, the authors opted for NiNPs deposited on LDH nanosheets, Ni/NiAl-LDH. In order to prove the advantage of the photo-thermal coupling, multiple experiments were performed: (i) under only light irradiation (UV-vis) no products were detected, (ii) while in the presence of an external heat source and UV-vis light, the H₂ production reached 407.51 $\mu\text{mol}\cdot\text{g}^{-1}\cdot\text{h}^{-1}$. At the same time, the catalyst exhibited UV, vis, and IR light absorption on a very broad range (between 220 and 2000 nm) owing to the SPR absorption properties of metallic NiNPs. These findings were confirmed not only by the optical characterizations performed but also with a (iii) third type of experiment, which involved the use of a Xe lamp and no external heat source. Herein, the surface temperature of the catalyst reached 671 K due to the outstanding absorption and conversion of IR light to heat energy of the Ni-containing catalysts [119]. Wang et al. focused their work on a system capable of undergoing photocatalytic water splitting reactions based upon N-doped Ti₃C₂ (N₁₀TC) MXene and NiFe-LDH. The remarkable results are attributed to the Schottky junction carrier trapping synergy created between the materials, thus a lower recombination rate, and the high capacity of the system to utilize the created plasmonic hot carriers [120].

6. Conclusions and Future Perspectives

This paper provides a comprehensive review on the design and fabrication of heterostructures of PNPs/LDH and their applications in the new field of hybrid plasmonic catalysis for energy related and environmental processes. As displayed by the results discussed in this review, the close conjunction and interplay of the heterostructured nano-units created plasmonic/non-plasmonic catalytic interfaces with functions that emerge from synergistically enhanced and complementary physicochemical features of the components. LDH, in their pristine form or transformed in mixed metal oxides, are endowed with advantageous features, e.g., harvesting all range of solar radiation via compositional flexibility, highly dispersed MO₆ units, and O-H surface bonds via their unique layered structure and morphology, unique memory effect property, as well as the presence of both cations and anions, which both impact the catalytic performances. Thus, LDH acts not only to confine and stabilize PNPs within the layered porous matrix but is able to establish specific metal support interactions such that the light energy harvested by the PNPs will trigger catalysis by the manifestation of plasmon-induced charge separation effect (PICS), co-catalytic effect or nano-antenna effect. However, we found that the field of plasmonic hybrid catalysis by using PNPs/LDH based heterostructures is still largely underexplored and information on PNPs/LDHs catalysts remains scarce despite that the development of high performant plasmonic heterostructures would have a strong impact on fabricating performant devices that rely on applications of plasmonic catalysis to create a sustainable society.

Several challenges remain in the development of plasmonic metal/LDH heterostructures and their application in the field of hybrid plasmonic catalysis, and we hope that these highlights will serve as a further guidance to future research.

First, controlled synthesis and design of the plasmonic metal/LDH heterostructures requires sustained research efforts in the future, focusing on both PNPs and LDH support counterparts, in terms of composition, control of particle structure and size, as well as surface/interface interactions. Obtaining high performant plasmonic nanostructures will continue to require the improvement of synthetic procedures and synthetic challenges to establish PNPs/support heteronanocomposites with high precision to tune targeted characteristics and, furthermore, to find how these characteristics are entangled to harvest the plasmonic energy in the form of electronic excitations to perform catalysis. This is a necessary prerequisite for developing performant catalysts and needs to be addressed by future research.

Next, research efforts have to focus on enhancing the LSPR response by controlling the size, shape, and surrounding environment of the PNPs. Additionally, certain limitations are yet to be overcome regarding the stability of PNPs/LDH heterostructures and the preservation of their nanomorphology during catalysis.

Furthermore, more attempts are encouraged for going beyond laboratory trials and upscaling the PNPs/LDH synthesis for their demonstration and integration in larger scale applications. Larger scale synthesis was demonstrated for the LDH materials, although compositional aspects were not completely addressed, with examples for producing large scale batches of LDHs containing transitional metals that are key photocatalytic components, or multicomponent LDH systems. This has to be followed by the PNPs synthesis and their heterostructuring with LDHs, for which only synthesis at the laboratory scale was reported until present. It was well noted that two noble plasmonic metals, i.e., Au and Ag, were dominantly used for obtaining PNPs/LDHs heterostructures, although current experimental evidence suggests that more significant results have to be established for the fast-growing field of non-noble PNPs/LDH heterostructured catalysts. Taking into account the reduced prices and the straightforward recyclability characteristics of the non-noble metals, it is important to focus on the design of catalysts with higher loadings of active metals (MeNPs) without a great cost increase. At the same time, instead of higher loadings, the non-noble metallic plasmons may be used in tandem systems (bi-metallic or alloys) with noble metal plasmons in order to create a synergistic effect. In this way, the photoactivity is considerably increased while a reduced amount of noble metals is used. Moreover, the spectral range activity of MeNPs may be extended to the near infrared (NIR) region, assuring an extra 50% of the solar light usability.

It is further significant to develop PNPs/LDH heterostructure with strong plasmon resonance bands of LSPR by modulating the electron transfer between the nanounits. To move the field forward, we need to understand how the LDH multifunctionality can be used to increase the upper limits of the energetic charge carrier extraction from PNPs/LDH systems and how this energy is distributed within the heterostructured catalyst. Next, an important perspective would be to study and better understand the mechanism behind the photocatalysis involving PNPs/LDH.

It is anticipated that more significant results will happen in this fast growing field of plasmonic heterostructured catalysts involving the heterostructuring of PNPs with LDH. We hope that this work should serve as a motivation to achieve cutting-edge scientific results in the spectral and functional versatility of PNPs/LDH toward developing highly performant hybrid plasmonic devices for applications in catalysis.

Author Contributions: Conceptualization, G.C and P.C.; funding acquisition P.C.; writing—original draft preparation, E.M.S., R.G.C., D.G. and G.C.; writing—review and editing, D.G., E.M.S., P.C. and G.C.; visualization, P.C.; supervision P.C and G.C. All authors have read and agreed to the published version of the manuscript.

Funding: E.M.S. acknowledges the Fund for Scientific Research Flanders (FWO—Vlaanderen) for financial support. G.C. is grateful for the financial supports from the Grant-in-Aid for Scientific Research from Romanian National Authority for Scientific Research, CNCS-UEFISCDI (PN-II-ID-1751).

Data Availability Statement: Not applicable.

Conflicts of Interest: The authors declare no conflict of interest.

References

1. Brongersma, M.L.; Halas, N.J.; Nordlander, P. Plasmon-induced hot carrier science and technology. *Nat. Nanotechnol.* **2015**, *10*, 25–34. [[CrossRef](#)]
2. Brongersma, M.L.; Shalaev, V.M. Applied physics. The case for plasmonics. *Science* **2010**, *328*, 440–441. [[CrossRef](#)] [[PubMed](#)]
3. Clavero, C. Plasmon-induced hot-electron generation at nanoparticle/metal-oxide interfaces for photovoltaic and photocatalytic devices. *Nat. Photonics* **2014**, *8*, 95–103. [[CrossRef](#)]

4. Zhang, Y.; He, S.; Guo, W.; Hu, Y.; Huang, J.; Mulcahy, J.R.; Wei, W.D. Surface-Plasmon-Driven Hot Electron Photochemistry. *Chem. Rev.* **2018**, *118*, 2927–2954. [[CrossRef](#)] [[PubMed](#)]
5. King, M.E.; Fonseca Guzman, M.V.; Ross, M.B. Material strategies for function enhancement in plasmonic architectures. *Nanoscale* **2022**, *14*, 602–611. [[CrossRef](#)]
6. Van Deelen, T.W.; Hernández Mejía, C.; de Jong, K.P. Control of metal-support interactions in heterogeneous catalysts to enhance activity and selectivity. *Nat. Catal.* **2019**, *2*, 955–970. [[CrossRef](#)]
7. Han, B.; Guo, Y.; Huang, Y.; Xi, W.; Xu, J.; Luo, J.; Qi, H.; Ren, Y.; Liu, X.; Qiao, B.; et al. Strong Metal-Support Interactions between Pt Single Atoms and TiO₂. *Angew. Chem. Int. Ed. Engl.* **2020**, *59*, 11824–11829. [[CrossRef](#)] [[PubMed](#)]
8. Hashemi, F.S.; Grillo, F.; Ravikumar, V.R.; Benz, D.; Shekhar, A.; Griffiths, M.B.; Barry, S.T.; Van Ommen, J.R. Thermal Atomic Layer Deposition of Gold Nanoparticles: Controlled Growth and Size Selection for Photocatalysis. *Nanoscale* **2020**, *12*, 9005–9013. [[CrossRef](#)]
9. Sayed, M.; Yu, J.; Liu, G.; Jaroniec, M. Non-Noble Plasmonic Metal-Based Photocatalysts. *Chem. Rev.* **2022**, *122*, 10484–10537. [[CrossRef](#)]
10. Linic, S.; Christopher, P.; Ingram, D.B. Plasmonic-metal nanostructures for efficient conversion of solar to chemical energy. *Nat. Mater.* **2011**, *10*, 911–921. [[CrossRef](#)]
11. Chavez, S.; Aslam, U.; Linic, S. Design Principles for Directing Energy and Energetic Charge Flow in Multicomponent Plasmonic Nanostructures. *ACS Energy Lett.* **2018**, *3*, 1590–1596. [[CrossRef](#)]
12. Carja, G.; Birsanu, M.; Okada, K.; Garcia, H. Composite plasmonic gold/layered double hydroxides and derived mixed oxides as novel photocatalysts for hydrogen generation under solar irradiation. *J. Mater. Chem. A* **2013**, *1*, 9092–9098. [[CrossRef](#)]
13. Ukharty, M.S.; Saito, R. Surface plasmons in graphene and carbon nanotubes. *Carbon* **2020**, *167*, 455–474. [[CrossRef](#)]
14. Xiao, J.D.; Han, L.; Luo, J.; Yu, S.H.; Jiang, H.L. Integration of Plasmonic Effects and Schottky Junctions into Metal-Organic Framework Composites: Steering Charge Flow for Enhanced Visible-Light Photocatalysis. *Angew. Chem. Int. Ed. Engl.* **2018**, *57*, 1103–1107. [[CrossRef](#)]
15. Kale, M.J.; Avanesian, T.; Christopher, P. Direct Photocatalysis by Plasmonic Nanostructures. *ACS Catal.* **2013**, *4*, 116–128. [[CrossRef](#)]
16. Cushing, S.K.; Li, J.; Meng, F.; Senty, T.R.; Suri, S.; Zhi, M.; Li, M.; Bristow, A.D.; Wu, N. Photocatalytic activity enhanced by plasmonic resonant energy transfer from metal to semiconductor. *J. Am. Chem. Soc.* **2012**, *134*, 15033–15041. [[CrossRef](#)]
17. Rossi, T.P.; Shegai, T.; Erhart, P.; Antosiewicz, T.J. Strong plasmon-molecule coupling at the nanoscale revealed by first-principles modeling. *Nat. Commun.* **2019**, *10*, 3336. [[CrossRef](#)] [[PubMed](#)]
18. Wu, M.J.; Wu, J.Z.; Zhang, J.; Chen, H.; Zhou, J.Z.; Qian, G.R.; Xu, Z.P.; Du, Z.; Rao, Q.L. A review on fabricating heterostructures from layered double hydroxides for enhanced photocatalytic activities. *Catal. Sci. Technol.* **2018**, *8*, 1207–1228. [[CrossRef](#)]
19. Naldoni, A.; Riboni, F.; Guler, U.; Boltasseva, A.; Shalaev, V.M.; Kildishev, A.V. Solar-Powered Plasmon-Enhanced Heterogeneous Catalysis. *Nanophotonics* **2016**, *5*, 112–133. [[CrossRef](#)]
20. Tatsuma, T.; Nishi, H.; Ishida, T. Plasmon-induced charge separation: Chemistry and wide applications. *Chem. Sci.* **2017**, *8*, 3325–3337. [[CrossRef](#)] [[PubMed](#)]
21. Mohapatra, L.; Parida, K. A review on the recent progress, challenges and perspective of layered double hydroxides as promising photocatalysts. *J. Mater. Chem. A* **2016**, *4*, 10744–10766. [[CrossRef](#)]
22. Mao, F.; Hao, P.; Zhu, Y.; Kong, X.; Duan, X. Layered double hydroxides: Scale production and application in soil remediation as super-stable mineralizer. *Chin. J. Chem. Eng.* **2022**, *41*, 42–48. [[CrossRef](#)]
23. Kong, X.; Ge, R.; Liu, T.; Xu, S.; Hao, P.; Zhao, X.; Li, Z.; Lei, X.; Duan, H. Super-stable mineralization of cadmium by calcium-aluminum layered double hydroxide and its large-scale application in agriculture soil remediation. *Chem. Eng. J.* **2021**, *407*, 127178. [[CrossRef](#)]
24. Cavani, F.; Trifirò, F.; Vaccari, A. Hydrotalcite-type anionic clays: Preparation, properties and applications. *Catal. Today* **1991**, *11*, 173–301. [[CrossRef](#)]
25. Auerbach, S.M.; Carrado, K.A.; Dutta, P.K. *Handbook of Layered Materials*; CRC Press: New York, NY, USA, 2004; p. 664.
26. Britto, S.; Kamath, P.V. Polytypism in the lithium-aluminum layered double hydroxides: The [LiAl₂(OH)₆]⁺ layer as a structural synthon. *Inorg. Chem.* **2011**, *50*, 5619–5627. [[CrossRef](#)]
27. Zhang, T.; Li, Q.; Xiao, H.; Lu, H.; Zhou, Y. Synthesis of Li–Al Layered Double Hydroxides (LDHs) for Efficient Fluoride Removal. *Ind. Eng. Chem. Res.* **2012**, *51*, 11490–11498. [[CrossRef](#)]
28. Seftel, E.M.; Popovici, E.; Mertens, M.; Van Tendeloo, G.; Cool, P.; Vansant, E.F. The influence of the cationic ratio on the incorporation of Ti⁴⁺ in the brucite-like sheets of layered double hydroxides. *Microporous Mesoporous Mater.* **2008**, *111*, 12–17. [[CrossRef](#)]
29. Zhang, W.H.; Guo, X.D.; He, J.; Qian, Z.Y. Preparation of Ni(II)/Ti(IV) layered double hydroxide at high supersaturation. *J. Eur. Ceram. Soc.* **2008**, *28*, 1623–1629. [[CrossRef](#)]
30. Seftel, E.M.; Popovici, E.; Mertens, M.; Stefaniak, E.A.; Van Grieken, R.; Cool, P.; Vansant, E.F. SnIV-containing layered double hydroxides as precursors for nano-sized ZnO/SnO₂ photocatalysts. *Appl. Catal. B Environ.* **2008**, *84*, 699–705. [[CrossRef](#)]
31. Feng-Xian, L.I.U.; Zhe-Ming, N.I.; Sheng-Jie, X.I.A.; Jun-Hui, J.; Meng-Meng, S. Visible-light Photocatalytic Degradation Effect of Sn-Contained Layered Double Hydroxides on 4-Chlorophenol. *J. Inorg. Mater.* **2016**, *31*, 7–13. [[CrossRef](#)]

32. Gabriel, R.; Carvalho, S.H.V.d.; Duarte, J.L.d.S.; Oliveira, L.M.T.M.; Giannakoudakis, D.A.; Triantafyllidis, K.S.; Soletti, J.I.; Meili, L. Mixed metal oxides derived from layered double hydroxide as catalysts for biodiesel production. *Appl. Catal. A Gen.* **2022**, *630*, 118470. [[CrossRef](#)]
33. Razaq, A.; Ali, S.; Asif, M.; In, S.-I. Layered Double Hydroxide (LDH) Based Photocatalysts: An Outstanding Strategy for Efficient Photocatalytic CO₂ Conversion. *Catalysts* **2020**, *10*, 1185. [[CrossRef](#)]
34. Zhao, Y.; Jia, X.; Waterhouse, G.I.N.; Wu, L.-Z.; Tung, C.-H.; O'Hare, D.; Zhang, T. Layered Double Hydroxide Nanostructured Photocatalysts for Renewable Energy Production. *Adv. Energy Mater.* **2016**, *6*, 1501974. [[CrossRef](#)]
35. Silva, C.G.; Bouzidi, Y.; Fornés, V.; García, H. Layered Double Hydroxides as Highly Efficient Photocatalysts for Visible Light Oxygen Generation from Water. *J. Am. Chem. Soc.* **2009**, *131*, 13833–13839. [[CrossRef](#)]
36. Lestari, P.R.; Takei, T.; Yanagida, S.; Kumada, N. Facile and controllable synthesis of Zn-Al layered double hydroxide/silver hybrid by exfoliation process and its plasmonic photocatalytic activity of phenol degradation. *Mater. Chem. Phys.* **2020**, *250*, 122988. [[CrossRef](#)]
37. Gilea, D.; Radu, T.; Muresanu, M.; Carja, G. Plasmonic photocatalysts based on silver nanoparticles—layered double hydroxides for efficient removal of toxic compounds using solar light. *Appl. Surf. Sci.* **2018**, *444*, 407–413. [[CrossRef](#)]
38. Chen, C.R.; Zeng, H.Y.; Yi, M.Y.; Xiao, G.F.; Zhu, R.L.; Cao, X.J.; Shen, S.G.; Peng, J.W. Fabrication of Ag₂O/Ag decorated ZnAl-layered double hydroxide with enhanced visible light photocatalytic activity for tetracycline degradation. *Ecotoxicol. Environ. Saf.* **2019**, *172*, 423–431. [[CrossRef](#)]
39. Sobhana, L.; Sarakha, M.; Prevot, V.; Fardim, P. Layered double hydroxides decorated with Au-Pd nanoparticles to photodegrade Orange II from water. *Appl. Clay Sci.* **2016**, *134*, 120–127. [[CrossRef](#)]
40. Darie, M.; Seftel, E.M.; Mertens, M.; Ciocarlan, R.G.; Cool, P.; Carja, G. Harvesting solar light on a tandem of Pt or Pt-Ag nanoparticles on layered double hydroxides photocatalysts for p-nitrophenol degradation in water. *Appl. Clay Sci.* **2019**, *182*, 105250. [[CrossRef](#)]
41. Zhu, Y.; Zhu, R.; Zhu, G.; Wang, M.; Chen, Y.; Zhu, J.; Xi, Y.; He, H. Plasmonic Ag coated Zn/Ti-LDH with excellent photocatalytic activity. *Appl. Surf. Sci.* **2018**, *433*, 458–467. [[CrossRef](#)]
42. Fu, S.; Zheng, Y.; Zhou, X.; Ni, Z.; Xia, S. Visible light promoted degradation of gaseous volatile organic compounds catalyzed by Au supported layered double hydroxides: Influencing factors, kinetics and mechanism. *J. Hazard. Mater.* **2019**, *363*, 41–54. [[CrossRef](#)]
43. Mikami, G.; Grosu, F.; Kawamura, S.; Yoshida, Y.; Carja, G.; Izumi, Y. Harnessing self-supported Au nanoparticles on layered double hydroxides comprising Zn and Al for enhanced phenol decomposition under solar light. *Appl. Catal. B Environ.* **2016**, *199*, 260–271. [[CrossRef](#)]
44. Tian, L.; Zhao, Y.; He, S.; Wei, M.; Duan, X. Immobilized Cu–Cr layered double hydroxide films with visible-light responsive photocatalysis for organic pollutants. *Chem. Eng. J.* **2012**, *184*, 261–267. [[CrossRef](#)]
45. Seftel, E.M.; Puscasu, M.; Mertens, M.; Cool, P.; Carja, G. Photo-responsive behavior of γ -Fe₂O₃ NPs embedded into ZnAlFe-LDH matrices and their catalytic efficiency in wastewater remediation. *Catal. Today* **2015**, *252*, 7–13. [[CrossRef](#)]
46. Seftel, E.M.; Niarchos, M.; Mitropoulos, C.; Mertens, M.; Vansant, E.F.; Cool, P. Photocatalytic removal of phenol and methylene-blue in aqueous media using TiO₂@LDH clay nanocomposites. *Catal. Today* **2015**, *252*, 120–127. [[CrossRef](#)]
47. Yang, Z.-Z.; Zhang, C.; Zeng, G.-M.; Tan, X.-F.; Huang, D.-L.; Zhou, J.-W.; Fang, Q.-Z.; Yang, K.-H.; Wang, H.; Wei, J.; et al. State-of-the-art progress in the rational design of layered double hydroxide based photocatalysts for photocatalytic and photo-electrochemical H₂/O₂ production. *Coord. Chem. Rev.* **2021**, *446*, 214103. [[CrossRef](#)]
48. Parida, K.M.; Mohapatra, L. Carbonate intercalated Zn/Fe layered double hydroxide: A novel photocatalyst for the enhanced photo degradation of azo dyes. *Chem. Eng. J.* **2012**, *179*, 131–139. [[CrossRef](#)]
49. Mohapatra, L.; Parida, K.M. Zn–Cr layered double hydroxide: Visible light responsive photocatalyst for photocatalytic degradation of organic pollutants. *Sep. Purif. Technol.* **2012**, *91*, 73–80. [[CrossRef](#)]
50. Wang, K.; Zhang, L.; Su, Y.; Shao, D.; Zeng, S.; Wang, W. Photoreduction of carbon dioxide of atmospheric concentration to methane with water over CoAl-layered double hydroxide nanosheets. *J. Mater. Chem. A* **2018**, *6*, 8366–8373. [[CrossRef](#)]
51. Bai, S.; Wang, Z.; Tan, L.; Waterhouse, G.I.N.; Zhao, Y.; Song, Y.-F. 600 nm Irradiation-Induced Efficient Photocatalytic CO₂ Reduction by Ultrathin Layered Double Hydroxide Nanosheets. *Ind. Eng. Chem. Res.* **2020**, *59*, 5848–5857. [[CrossRef](#)]
52. Low, T.; Chaves, A.; Caldwell, J.D.; Kumar, A.; Fang, N.X.; Avouris, P.; Heinz, T.F.; Guinea, F.; Martin-Moreno, L.; Koppens, F. Polaritons in layered two-dimensional materials. *Nat. Mater.* **2017**, *16*, 182–194. [[CrossRef](#)]
53. Cortes, E.; Besteiro, L.V.; Alabastri, A.; Baldi, A.; Tagliabue, G.; Demetriadou, A.; Narang, P. Challenges in Plasmonic Catalysis. *ACS Nano* **2020**, *14*, 16202–16219. [[CrossRef](#)]
54. Ahmed, N.; Shibata, Y.; Taniguchi, T.; Izumi, Y. Photocatalytic conversion of carbon dioxide into methanol using zinc–copper–M(III) (M = aluminum, gallium) layered double hydroxides. *J. Catal.* **2011**, *279*, 123–135. [[CrossRef](#)]
55. Iguchi, S.; Teramura, K.; Hosokawa, S.; Tanaka, T. Effect of the chloride ion as a hole scavenger on the photocatalytic conversion of CO₂ in an aqueous solution over Ni-Al layered double hydroxides. *Phys. Chem. Chem. Phys.* **2015**, *17*, 17995–18003. [[CrossRef](#)]
56. Flores-Flores, M.; Luévano-Hipólito, E.; Martínez, L.M.T.; Morales-Mendoza, G.; Gómez, R. Photocatalytic CO₂ conversion by MgAl layered double hydroxides: Effect of Mg²⁺ precursor and microwave irradiation time. *J. Photochem. Photobiol. A Chem.* **2018**, *363*, 68–73. [[CrossRef](#)]

57. Puscasu, C.-M.; Seftel, E.M.; Mertens, M.; Cool, P.; Carja, G. ZnTiLDH and the Derived Mixed Oxides as Mesoporous Nanoarchitectonics with Photocatalytic Capabilities. *J. Inorg. Organomet. Polym. Mater.* **2014**, *25*, 259–266. [[CrossRef](#)]
58. Wang, Q.; O'Hare, D. Recent advances in the synthesis and application of layered double hydroxide (LDH) nanosheets. *Chem. Rev.* **2012**, *112*, 4124–4155. [[CrossRef](#)]
59. Ha, M.; Kim, J.H.; You, M.; Li, Q.; Fan, C.; Nam, J.M. Multicomponent Plasmonic Nanoparticles: From Heterostructured Nanoparticles to Colloidal Composite Nanostructures. *Chem. Rev.* **2019**, *119*, 12208–12278. [[CrossRef](#)]
60. Cobley, C.M.; Skrabalak, S.E.; Campbell, D.J.; Xia, Y. Shape-Controlled Synthesis of Silver Nanoparticles for Plasmonic and Sensing Applications. *Plasmonics* **2009**, *4*, 171–179. [[CrossRef](#)]
61. Koya, A.N.; Zhu, X.; Ohannesian, N.; Yanik, A.A.; Alabastri, A.; Proietti Zaccaria, R.; Krahn, R.; Shih, W.C.; Garoli, D. Nanoporous Metals: From Plasmonic Properties to Applications in Enhanced Spectroscopy and Photocatalysis. *ACS Nano* **2021**, *15*, 6038–6060. [[CrossRef](#)]
62. Cortie, M.B.; McDonagh, A.M. Synthesis and optical properties of hybrid and alloy plasmonic nanoparticles. *Chem. Rev.* **2011**, *111*, 3713–3735. [[CrossRef](#)]
63. Vinci, G.; Rapa, M. Noble Metal Nanoparticles Applications: Recent Trends in Food Control. *Bioengineering* **2019**, *6*, 10. [[CrossRef](#)]
64. Wang, R.; Shen, J.; Sun, K.; Tang, H.; Liu, Q. Enhancement in photocatalytic activity of CO₂ reduction to CH₄ by 0D/2D Au/TiO₂ plasmon heterojunction. *Appl. Surf. Sci.* **2019**, *493*, 1142–1149. [[CrossRef](#)]
65. Kunthakudee, N.; Puangpetch, T.; Ramakul, P.; Serivalsatit, K.; Hunsom, M. Light-assisted synthesis of Au/TiO₂ nanoparticles for H₂ production by photocatalytic water splitting. *Int. J. Hydrog. Energy* **2022**, *47*, 23570–23582. [[CrossRef](#)]
66. Chang, Y.; Liu, Z.; Shen, X.; Zhu, B.; Macharia, D.K.; Chen, Z.; Zhang, L. Synthesis of Au nanoparticle-decorated carbon nitride nanorods with plasmon-enhanced photoabsorption and photocatalytic activity for removing various pollutants from water. *J. Hazard. Mater.* **2018**, *344*, 1188–1197. [[CrossRef](#)]
67. Kashyap, T.; Biswasi, S.; Pal, A.R.; Choudhury, B. Unraveling the Catalytic and Plasmonic Roles of g-C₃N₄ Supported Ag and Au Nanoparticles Under Selective Photoexcitation. *ACS Sustain. Chem. Eng.* **2019**, *7*, 19295–19302. [[CrossRef](#)]
68. Yang, F.; Du, M.; Yin, K.; Qiu, Z.; Zhao, J.; Liu, C.; Zhang, G.; Gao, Y.; Pang, H. Applications of Metal-Organic Frameworks in Water Treatment: A Review. *Small* **2022**, *18*, 2105715. [[CrossRef](#)]
69. Liang, R.; Jing, F.; Shen, L.; Qin, N.; Wu, L. M@MIL-100(Fe) (M = Au, Pd, Pt) nanocomposites fabricated by a facile photodeposition process: Efficient visible-light photocatalysts for redox reactions in water. *Nano Res.* **2015**, *8*, 3237–3249. [[CrossRef](#)]
70. Cure, J.; Mattson, E.; Cocq, K.; Assi, H.; Jensen, S.; Tan, K.; Catalano, M.; Yuan, S.; Wang, H.; Feng, L.; et al. High stability of ultra-small and isolated gold nanoparticles in metal-organic framework materials. *J. Mater. Chem. A* **2019**, *7*, 17536–17546. [[CrossRef](#)]
71. Stucchi, M.; Bianchi, C.L.; Argiris, C.; Pifferi, V.; Neppolian, B.; Cerrato, G.; Boffito, D.C. Ultrasound assisted synthesis of Ag-decorated TiO₂ active in visible light. *Ultrason. Sonochem* **2018**, *40*, 282–288. [[CrossRef](#)]
72. Rabhi, S.; Mahtout, L.; Bououdina, M.; Khezami, L.; Belkacemi, H.; Kerrami, A.; Sakher, E. Tuning the photocatalytic activity of TiO₂ by Ag loading: Experimental and modelling studies for the degradation of amlodipine besylate drug. *Ceram. Int.* **2021**, *47*, 21509–21521. [[CrossRef](#)]
73. Cruz, D.; Ortiz-Oliveros, H.B.; Flores-Espinosa, R.M.; Ávila Pérez, P.; Ruiz-López, I.I.; Quiroz-Estrada, K.F. Synthesis of Ag/TiO₂ composites by combustion modified and subsequent use in the photocatalytic degradation of dyes. *J. King Saud Univ.—Sci.* **2022**, *34*, 101966. [[CrossRef](#)]
74. Chen, M.; Guo, C.; Hou, S.; Wu, L.; Lv, J.; Hu, C.; Zhang, Y.; Xu, J. In-situ fabrication of Ag/P-g-C₃N₄ composites with enhanced photocatalytic activity for sulfamethoxazole degradation. *J. Hazard. Mater.* **2019**, *366*, 219–228. [[CrossRef](#)]
75. Narkbuakaew, T.; Sattayaporn, S.; Saito, N.; Sujaridworakun, P. Investigation of the Ag species and synergy of Ag-TiO₂ and g-C₃N₄ for the enhancement of photocatalytic activity under UV-Visible light irradiation. *Appl. Surf. Sci.* **2022**, *573*, 151617. [[CrossRef](#)]
76. Guo, F.; Yang, S.; Liu, Y.; Wang, P.; Huang, J.; Sun, W.-Y. Size Engineering of Metal-Organic Framework MIL-101(Cr)-Ag Hybrids for Photocatalytic CO₂ Reduction. *ACS Catal.* **2019**, *9*, 8464–8470. [[CrossRef](#)]
77. Hayati, P.; Mehrabadi, Z.; Karimi, M.; Janczak, J.; Mohammadi, K.; Mahmoudi, G.; Dadi, F.; Fard, M.J.S.; Hasanzadeh, A.; Rostamnia, S. Photocatalytic activity of new nanostructures of an Ag(i) metal-organic framework (Ag-MOF) for the efficient degradation of MCPA and 2,4-D herbicides under sunlight irradiation. *New J. Chem.* **2021**, *45*, 3408–3417. [[CrossRef](#)]
78. Caswell, T.; Dlamini, M.W.; Miedziak, P.J.; Pattison, S.; Davies, P.R.; Taylor, S.H.; Hutchings, G.J. Enhancement in the rate of nitrate degradation on Au- and Ag-decorated TiO₂ photocatalysts. *Catal. Sci. Technol.* **2020**, *10*, 2082–2091. [[CrossRef](#)]
79. Kashyap, T.; Biswas, S.; Ahmed, S.; Kalita, D.; Nath, P.; Choudhury, B. Plasmon activation versus plasmon quenching on the overall photocatalytic performance of Ag/Au bimetal decorated g-C₃N₄ nanosheets under selective photoexcitation: A mechanistic understanding with experiment and theory. *Appl. Catal. B Environ.* **2021**, *298*, 120614. [[CrossRef](#)]
80. Yang, X.; Wang, Y.; Zhang, L.; Fu, H.; He, P.; Han, D.; Lawson, T.; An, X. The Use of Tunable Optical Absorption Plasmonic Au and Ag Decorated TiO₂ Structures as Efficient Visible Light Photocatalysts. *Catalysts* **2020**, *10*, 139. [[CrossRef](#)]
81. Kim, S.; Kim, J.M.; Park, J.E.; Nam, J.M. Nonnoble-Metal-Based Plasmonic Nanomaterials: Recent Advances and Future Perspectives. *Adv. Mater.* **2018**, *30*, e1704528. [[CrossRef](#)]
82. Wei, D.; Tan, Y.; Wang, Y.; Kong, T.; Shen, S.; Mao, S.S. Function-switchable metal/semiconductor junction enables efficient photocatalytic overall water splitting with selective water oxidation products. *Sci. Bull.* **2020**, *65*, 1389–1395. [[CrossRef](#)]

83. DeSario, P.A.; Gordon, W.O.; Balboa, A.; Pennington, A.M.; Pitman, C.L.; McEntee, M.; Pietron, J.J. Photoenhanced Degradation of Sarin at Cu/TiO₂ Composite Aerogels: Roles of Bandgap Excitation and Surface Plasmon Excitation. *ACS Appl. Mater. Interfaces* **2021**, *13*, 12550–12561. [[CrossRef](#)]
84. Dai, B.; Zhao, W.; Huang, H.; Li, S.; Yang, G.; Wu, H.; Sun, C.; Leung, D.Y.C. Constructing an ohmic junction of copper@ cuprous oxide nanocomposite with plasmonic enhancement for photocatalysis. *J. Colloid Interface Sci.* **2022**, *616*, 163–176. [[CrossRef](#)]
85. Chen, B.; Zhang, J.; Yu, J.; Wang, R.; He, B.; Jin, J.; Wang, H.; Gong, Y. Rational design of all-solid-state TiO₂-x/Cu/ZnO Z-scheme heterojunction via ALD-assistance for enhanced photocatalytic activity. *J. Colloid Interface Sci.* **2022**, *607*, 760–768. [[CrossRef](#)]
86. Xu, B.; Zhang, H.; Baran, P.; Matras-Postolek, K.; Yang, P. Cu nanocrystals enhanced charge separation and transfer in superior thin g-C₃N₄ nanosheets. *J. Alloy. Compd.* **2022**, *919*, 165892. [[CrossRef](#)]
87. Xiao, L.; Zhang, Q.; Chen, P.; Chen, L.; Ding, F.; Tang, J.; Li, Y.-J.; Au, C.-T.; Yin, S.-F. Copper-mediated metal-organic framework as efficient photocatalyst for the partial oxidation of aromatic alcohols under visible-light irradiation: Synergism of plasmonic effect and schottky junction. *Appl. Catal. B Environ.* **2019**, *248*, 380–387. [[CrossRef](#)]
88. Yu, Y.; Dong, X.; Chen, P.; Geng, Q.; Wang, H.; Li, J.; Zhou, Y.; Dong, F. Synergistic Effect of Cu Single Atoms and Au-Cu Alloy Nanoparticles on TiO₂ for Efficient CO₂ Photoreduction. *ACS Nano* **2021**, *15*, 14453–14464. [[CrossRef](#)]
89. Babu, P.; Dash, S.R.; Behera, A.; Vijayaraghavan, T.; Ashok, A.; Parida, K. Prominence of Cu in a plasmonic Cu–Ag alloy decorated SiO₂@S-doped C₃N₄ core–shell nanostructured photocatalyst towards enhanced visible light activity. *Nanoscale Adv.* **2022**, *4*, 150–162. [[CrossRef](#)]
90. He, S.; Huang, J.; Goodsell, J.L.; Angerhofer, A.; Wei, W.D. Plasmonic Nickel-TiO₂ Heterostructures for Visible-Light-Driven Photochemical Reactions. *Angew. Chem. Int. Ed. Engl.* **2019**, *58*, 6038–6041. [[CrossRef](#)]
91. Wang, C.-C.; Chou, P.-H.; Yu, Y.-H.; Kei, C.-C. Deposition of Ni nanoparticles on black TiO₂ nanowire arrays for photoelectrochemical water splitting by atomic layer deposition. *Electrochim. Acta* **2018**, *284*, 211–219. [[CrossRef](#)]
92. Tudu, B.; Nalajala, N.; Saikia, P.; Gopinath, C.S. Cu–Ni Bimetal Integrated TiO₂ Thin Film for Enhanced Solar Hydrogen Generation. *Solar RRL* **2020**, *4*, 1900557. [[CrossRef](#)]
93. Naresh, G.; Kumar, V.; Sasikumar, B.; Venugopal, A. Improved H₂ yields over Cu-Ni-TiO₂ under solar light irradiation: Behaviour of alloy nano particles on photocatalytic H₂O splitting. *Appl. Catal. B Environ.* **2021**, *299*, 120654. [[CrossRef](#)]
94. Xu, M.; Wei, M. Layered Double Hydroxide-Based Catalysts: Recent Advances in Preparation, Structure, and Applications. *Adv. Funct. Mater.* **2018**, *28*, 1802943. [[CrossRef](#)]
95. Zecevic, J.; Vanbutsele, G.; de Jong, K.P.; Martens, J.A. Nanoscale intimacy in bifunctional catalysts for selective conversion of hydrocarbons. *Nature* **2015**, *528*, 245–248. [[CrossRef](#)]
96. Cadars, S.; Layrac, G.; Gérardin, C.; Deschamps, M.; Yates, J.R.; Tichit, D.; Massiot, D. Identification and Quantification of Defects in the Cation Ordering in Mg/Al Layered Double Hydroxides. *Chem. Mater.* **2011**, *23*, 2821–2831. [[CrossRef](#)]
97. Yang, Y.; Ren, Z.; Zhou, S.; Wei, M. Perspectives on Multifunctional Catalysts Derived from Layered Double Hydroxides toward Upgrading Reactions of Biomass Resources. *ACS Catal.* **2021**, *11*, 6440–6454. [[CrossRef](#)]
98. Aslam, U.; Rao, V.G.; Chavez, S.; Linic, S. Catalytic conversion of solar to chemical energy on plasmonic metal nanostructures. *Nat. Catal.* **2018**, *1*, 656–665. [[CrossRef](#)]
99. Zhang, F.; Zhao, X.; Feng, C.; Li, B.; Chen, T.; Lu, W.; Lei, X.; Xu, S. Crystal-Face-Selective Supporting of Gold Nanoparticles on Layered Double Hydroxide as Efficient Catalyst for Epoxidation of Styrene. *ACS Catal.* **2011**, *1*, 232–237. [[CrossRef](#)]
100. Varade, D.; Haraguchi, K. Efficient approach for preparing gold nanoparticles in layered double hydroxide: Synthesis, structure, and properties. *J. Mater. Chem.* **2012**, *22*, 17649–17655. [[CrossRef](#)]
101. Mitsudome, T.; Noujima, A.; Mizugaki, T.; Jitsukawa, K.; Kaneda, K. Supported gold nanoparticles as a reusable catalyst for synthesis of lactones from diols using molecular oxygen as an oxidant under mild conditions. *Green Chem.* **2009**, *11*, 793–797. [[CrossRef](#)]
102. Mitsudome, T.; Noujima, A.; Mizugaki, T.; Jitsukawa, K.; Kaneda, K. Efficient Aerobic Oxidation of Alcohols using a Hydrotalcite-Supported Gold Nanoparticle Catalyst. *Adv. Synth. Catal.* **2009**, *351*, 1890–1896. [[CrossRef](#)]
103. Liu, P.; Degirmenci, V.; Hensen, E.J.M. Unraveling the synergy between gold nanoparticles and chromium-hydrotalcites in aerobic oxidation of alcohols. *J. Catal.* **2014**, *313*, 80–91. [[CrossRef](#)]
104. Gupta, N.K.; Nishimura, S.; Takagaki, A.; Ebitani, K. Hydrotalcite-supported gold-nanoparticle-catalyzed highly efficient base-free aqueous oxidation of 5-hydroxymethylfurfural into 2,5-furandicarboxylic acid under atmospheric oxygen pressure. *Green Chem.* **2011**, *13*, 824–827. [[CrossRef](#)]
105. Noujima, A.; Mitsudome, T.; Mizugaki, T.; Jitsukawa, K.; Kaneda, K. Selective deoxygenation of epoxides to alkenes with molecular hydrogen using a hydrotalcite-supported gold catalyst: A concerted effect between gold nanoparticles and basic sites on a support. *Angew. Chem. Int. Ed. Engl.* **2011**, *50*, 2986–2989. [[CrossRef](#)]
106. Yang, Z.-Z.; Zhang, C.; Zeng, G.-M.; Tan, X.-F.; Wang, H.; Huang, D.-L.; Yang, K.-H.; Wei, J.-J.; Ma, C.; Nie, K. Design and engineering of layered double hydroxide based catalysts for water depollution by advanced oxidation processes: A review. *J. Mater. Chem. A* **2020**, *8*, 4141–4173. [[CrossRef](#)]
107. Xiao, Q.; Liu, Z.; Wang, F.; Sarina, S.; Zhu, H. Tuning the reduction power of visible-light photocatalysts of gold nanoparticles for selective reduction of nitroaromatics to azoxy-compounds—Tailoring the catalyst support. *Appl. Catal. B Environ.* **2017**, *209*, 69–79. [[CrossRef](#)]

108. Arnob, M.M.P.; Artur, C.; Misbah, I.; Mubeen, S.; Shih, W.C. 10x-Enhanced Heterogeneous Nanocatalysis on a Nanoporous Gold Disk Array with High-Density Hot Spots. *ACS Appl. Mater. Interfaces* **2019**, *11*, 13499–13506. [[CrossRef](#)]
109. Ao, Y.; Wang, D.; Wang, P.; Wang, C.; Hou, J.; Qian, J. Enhanced photocatalytic properties of the 3D flower-like Mg-Al layered double hydroxides decorated with Ag₂CO₃ under visible light illumination. *Mater. Res. Bull.* **2016**, *80*, 23–29. [[CrossRef](#)]
110. Tonda, S.; Jo, W.-K. Plasmonic Ag nanoparticles decorated NiAl-layered double hydroxide/graphitic carbon nitride nanocomposites for efficient visible-light-driven photocatalytic removal of aqueous organic pollutants. *Catal. Today* **2018**, *315*, 213–222. [[CrossRef](#)]
111. Fujiwara, K.; Okuyama, K.; Pratsinis, S.E. Metal–support interactions in catalysts for environmental remediation. *Environ. Sci. Nano* **2017**, *4*, 2076–2092. [[CrossRef](#)]
112. Sahoo, D.P.; Patnaik, S.; Rath, D.; Mohapatra, P.; Mohanty, A.; Parida, K. Influence of Au/Pd alloy on an amine functionalised ZnCr LDH–MCM-41 nanocomposite: A visible light sensitive photocatalyst towards one-pot imine synthesis. *Catal. Sci. Technol.* **2019**, *9*, 2493–2513. [[CrossRef](#)]
113. Park, J.-E.; Kim, M.; Hwang, J.-H.; Nam, J.-M. Golden Opportunities: Plasmonic Gold Nanostructures for Biomedical Applications based on the Second Near-Infrared Window. *Small Methods* **2017**, *1*, 1600032. [[CrossRef](#)]
114. Ma, J.; Ding, J.; Li, L.; Zou, J.; Kong, Y.; Komarneni, S. In situ reduction for synthesis of nano-sized Cu₂O particles on MgCuAl-LDH layers for degradation of orange II under visible light. *Ceram. Int.* **2015**, *41*, 3191–3196. [[CrossRef](#)]
115. Carja, G.; Dartu, L.; Okada, K.; Fortunato, E. Nanoparticles of copper oxide on layered double hydroxides and the derived solid solutions as wide spectrum active nano-photocatalysts. *Chem. Eng. J.* **2013**, *222*, 60–66. [[CrossRef](#)]
116. Wang, X.; Wang, R.; Wang, J.; Fan, C.; Zheng, Z. The synergistic role of the support surface and Au-Cu alloys in a plasmonic Au-Cu@LDH photocatalyst for the oxidative esterification of benzyl alcohol with methanol. *Phys. Chem. Chem. Phys.* **2020**, *22*, 1655–1664. [[CrossRef](#)]
117. Liu, H.; Dao, T.D.; Liu, L.; Meng, X.; Nagao, T.; Ye, J. Light assisted CO₂ reduction with methane over group VIII metals: Universality of metal localized surface plasmon resonance in reactant activation. *Appl. Catal. B Environ.* **2017**, *209*, 183–189. [[CrossRef](#)]
118. Carja, G.; Husanu, E.; Gherasim, C.; Iovu, H. Layered double hydroxides reconstructed in NiSO₄ aqueous solution as highly efficient photocatalysts for degrading two industrial dyes. *Appl. Catal. B Environ.* **2011**, *107*, 253–259. [[CrossRef](#)]
119. Li, T.; Tan, L.; Zhao, Y.; Song, Y.-F. Solar-driven hydrogen production from steam methane reforming using highly dispersed metallic Ni catalysts supported on layered double hydroxide nanosheets. *Chem. Eng. Sci.* **2021**, *245*, 116839. [[CrossRef](#)]
120. Wang, J.; Wei, X.; Song, W.; Shi, X.; Wang, X.; Zhong, W.; Wang, M.; Ju, J.; Tang, Y. Plasmonic Enhancement in Water Splitting Performance for NiFe Layered Double Hydroxide-N10 TC MXene Heterojunction. *ChemSusChem* **2021**, *14*, 1948–1954. [[CrossRef](#)]